PARTICLES IN A LINEARLY STRATIFIED FLUID

A Thesis

Submitted to the Faculty

of

Purdue University

by

Khushal Ashok Bhatija

In Partial Fulfillment of the

Requirements for the Degree

of

Master of Science

December 2019

Purdue University

West Lafayette, Indiana

THE PURDUE UNIVERSITY GRADUATE SCHOOL
STATEMENT OF THESIS APPROVAL

Dr. Arezoo Ardekani, Co-chair

School of Mechanical Engineering, Purdue University

Dr. Matthieu Mercier, Co-chair

Institut de Mécanique des Fluides de Toulouse, France

Dr. Sadegh Dabiri

School of Mechanical Engineering, Purdue University

Dr. Jun Chen

School of Mechanical Engineering, Purdue University

Approved by:

Dr. Jay P. Gore

Head of the School Graduate Program

ACKNOWLEDGMENTS

I would like to thank my thesis advisor Dr. Arezoo Ardekani for her support during my research. I am grateful for the flexibility she offered during the entirety of my program at Purdue University. I would like to thank Dr. Matthieu Mercier, my co-advisor for the opportunity to conduct experiments at IMFT. I would like to thank my committee members Dr. Sadegh Dabiri and Dr. Jun Chen for their valuable time. I would like to thank my parents, my sister and my grandmother for the emotional and mental support. Last but not the least I would like to thank all the lab members and my friends for their help and support in making graduate school an enjoyable experience.

TABLE OF CONTENTS

Page

LIST OF TABLES

LIST OF FIGURES

Figure Page

SYMBOLS

$\frac{D}{Dt}$	material derivative
ω	vorticity
$\mathbf{u}$	velocity vector
∇	vector differential operator
μ	dynamic viscosity of the fluid
ρ	density
p	pressure
Re	Reynolds number
Fr	Froude number
Pr	Prandtl number
N	Brunt-Väisälä frequency
g	acceleration due to gravity
ρ_0	average density of the fluid
a	characteristic length
V	settling speed of a particle
ν	kinematic viscosity of the fluid
κ	thermal diffusivity of the fluid
l_s	stratification length scale
Ri	Richardson number
α_d	constant in normalized drag coefficient equation
β	constant in normalized drag coefficient equation
t	time
x, y, z	Cartesian coordinates
a	diameter

L	length of cylindrical objects used in experiments
ρ_p	density of particles used in experiments
ρ^0	density of fresh water used during intensity calibration
I	Intensity of pixel of interest
I_0	Intensity of pixel of interest during calibration with fresh water
A	density-intensity calibration coefficient
B	density-intensity calibration coefficient
C	density-intensity calibration coefficient
R^2	coefficient of determination
ΔX	absolute uncertainty in any independent variable, X
I_{max}	maximum camera noise in an image
∂	partial derivative
$\tilde{R}$	discriminant of the quadratic density-intensity calibration law
U_r	ratio of particle speed at any z to the speed at which it enters the field of view
N_p	number of particles
U_s	time-average velocity of a 1 particle
U_p	time-average mean velocity of particles of N_p particles
U_s	time
α	percentage of density field disturbed
α_1	percentage of density field disturbed by 1 particle
α_p	percentage of density field disturbed by N_p particles
E_t	total potential energy
E_b	background potential energy
E_a	available potential energy
H	height of the imaging window
A_c	area of cross section of the portion of tank in the imaging window
N_x	number of divisions in the image along x for energy calculations
$\rho(z)$	unsorted density profile

ρ_m	minimum value of ρ in $\rho(z)$
ρ_M	maximum value of ρ in $\rho(z)$
$P(\tilde{\rho})$	probability density function of $\rho(z)$
Z_r	z location of a fluid packet after adiabatic sorting
$\rho(Z_r)$	sorted density profile
η	ratio of change in E_t to E_t before an experiment

ABSTRACT

Ashok Bhatija, Khushal M.S., Purdue University, December 2019. Particles in a Linearly Stratified Fluid. Major Professors: Arezoo Ardekani, Matthieu Mercier.

The settling of spherical and cylindrical particles in a linearly stratified fluid is investigated using experiments. The double-tank method is used to generate a linear stratification with a red colored dye homogeneously mixed in the heavy water tank. As a result of feeding the stratification using dyed heavy water, the concentration of dye varies with depth in the experiment tank. A powerful back-light and a digital camera are used to record the events. Assuming the concentration of dye is directly proportional to density of fluid, Beer-Lambert's law is used to generate a calibration between intensity of the light measured by the camera and density of the fluid. Using this calibration, density is evaluated in all the images captured. In the parameter space of this study, the spheres have three different wake patterns. The area of fluid disturbed by a suspension of spheres increases with Re and Fr. As a result, the amount of energy available for the mixing and the irreversible change of total potential energy in the system increases with Re, Fr and number of particles. Cylinders drag volumes of light fluid to larger depths in their wake than spheres and shed the light fluid in the form of vortices. This results in lower volumes of fluid perturbed by the cylinders. However, as the light fluid is dragged to larger depths, the amount of energy generated for mixing and the change in total potential energy of the system is higher. Spheres are thus more efficient in disturbing volumes of fluid but cylinders are more efficient in causing irreversible changes to the state of the system.

1. INTRODUCTION

Particles settling or rising in a fluid frequently occur in oceanography, chemical and energy industry. In many situations the particles travel through regions of density stratified fluids. Motion of translating particles is affected by the density stratification as the hydrodynamic forces acting on the particle are modified. The translating particles also affect the fluid domain by dragging light fluid to regions of heavy fluid (and vice versa). An understanding of the effects of stratification on particle motion and those of the particle on the density field is necessary to understand many environmental and industrial processes.

The ocean is made up of three primary layers namely the surface layer, thermocline and the deep ocean. The surface layer (up to 200 m deep) actively interacts with the atmosphere encountering winds from the air currents, heat fluxes from the sun's radiation resulting in turbulent mixing, evaporation and salinity gradients. The deep ocean is the part of ocean far away from the surface interactions and thus is much colder and denser. The thermocline is a stratified layer where the density of the ocean transitions from the light fluid in the surface layer to the heavy fluid in the deep ocean. Thickness of the pycnocline depends on the salinity and temperature of the surface layer which is affected by factors like latitude and climate. The pycnoclines are also hot spots where biological activity peaks, e.g., algae bloom formation occurs. The phytoplankton, consume the dissolved carbon dioxide for photosynthesis, forming a 'biological pump' for carbon dioxide from the ocean surface to the bottom of the ocean. The stable stratification through which these organisms move, affects the direction and extent of their motion, finding implications in marine biology [1, 2]. Swimming of marine organisms can also generate local mixing around them, affecting the nutrient consumption [3, 4].

Rising bubbles are used across multiple engineering applications. In the extraction of steel, bubbles rise through a thermally stratified melt to pick up non-metallic impurities and transfer them to the slag at the top. Knowledge of constitutive models estimating local, micro-scale mixing induced by these bubbles to the molten steel is still incomplete. These models are also of relevance in chemical and biological reactors which use the mixing caused by bubbles as an alternative to mechanical stirring [5].

Recent advances in geophysics [6] postulate that a possible trigger mechanism behind volcanoes which are caused by mixing of acidic and basic magmas, could be the mixing induced between these two layers of different density by the solid crystalline particles settling through them. In astrophysics, the means of energy transport from supermassive black holes and intracluster media is unknown. There exists a temperature stratification between the high-temperature intracluster medium which is at the boundary of the galaxy and its relatively cold core. Recent work [7] suggests that the transport of relativistic plasma bubbles from the galaxy core, through the stratification is responsible for the energy transport. In all of the fore-mentioned applications, information about the dynamics of particles travelling through a stratified fluid is necessary to bring closure to the problems. Details of recent advances in the field are given in these two review articles [1, 8]

1.1 Disturbances in stratified flows

Let us consider an initially static plane of fluid particles perpendicular to the direction of motion of a settling object. As the object translates and moves across the plane of fluid particles, it displaces them. The volume of fluid between the envelope of displaced particles and the initial plane after the object has translated an infinite distance is called the drift volume. The inertia of the drift volume is modeled as an added mass to the system known as virtual mass. Darwin [9] showed that for a cylinder and a sphere translating in a homogeneous fluid medium the ratio of the virtual mass to the mass of the fluid displaced is equal to the ratio of the drift volume

and the volume of the particle. Although it has been shown [10] that this equality is valid only for an infinitesimal particle, initially located at an infinite distance from the reference plane used to determine the drift volume, the existence of a relation between the drift volume and added mass provides a tool to indirectly quantify the hydrodynamic force exerted on the object by the fluid. The translating object also drags in its wake, some amount of the displaced fluid . This phenomenon is called entrainment. Unlike the case of homogeneous fluids, in stratified fluids, there exists a difference in fluid density upstream and downstream of the object which also modifies the hydrodynamic force experienced by the translating object.

Along with displacing and entraining fluid, a translating object also induces a pressure field in the domain. An isopycnal is defined as a surface of constant fluid density. In the case of a stratified fluid, apart from the pressure field, the body also generates local density gradients as it distorts isopycnals. Misalignment between the induced pressure and density gradients results in generation of vorticity. Equation 1.1 represents the vorticity equation for a stratified fluid where the first two terms are due to the induced pressure field and the third term, called the baroclinic torque, is induced by the density gradients [2]

$$\frac{D\omega}{Dt} = \omega.\nabla\mathbf{u} - \nabla \times \left(\frac{\mu}{\rho}\nabla \times \omega\right) + \frac{\nabla\rho}{\rho^2} \times \nabla p, \tag{1.1}$$

where ω is the vorticity, $\mathbf{u}$ is the velocity vector, $\frac{D}{Dt}$ is the material derivative, μ is the viscosity of the fluid, ρ is the density of the fluid, p is the pressure. The discussion of flow field using the baroclinic vorticity generation in the wake of a settling sphere in a stratified fluid was first given by [2] in the case of a constant viscosity fluid. Later, [11] compared the contributions of vorticity and buoyancy effects to the force acting on the settling spherical particle.

When there are no external disturbances, the mode of mass transport in a stratified fluid, is molecular diffusion from regions of high concentration to regions of low concentration. The evolution of a system from an initially non-homogeneous state to a state of homogeneity is called mixing. Stirring is the process by which the system is

agitated to achieve mixing. Stirring aids molecular diffusion by increasing the concentration gradients and surface area of diffusion. When an object translates through a stratified fluid, stirs it, through the processes of fluid displacement, fluid entrainment and generation of vorticity, thus aiding the mass transport. Quantifying the amount of mixing caused by stirring due to translating bodies is the information necessary to bring closure to above-mentioned problems.

1.2 Dimensionless parameters of interest

As discussed above, a particle translating in a stratified fluid results in momentum transport due to inertia, buoyancy and viscous effects and mass transport by enhancing diffusion. The dimensionless parameters characterizing mass and momentum transport in stratified fluids are the Reynolds number, Re, which is a ratio of inertial and viscous forces, the Froude number, Fr, which is a ratio of inertial and buoyancy forces and the Prandtl number, Pr which is a ratio of momentum and thermal diffusion.

In a stably stratified medium, when fluid is vertically displaced, it oscillates. If the resulting changes in density are small, the Boussinesq approximation is valid. The Brunt-Väisälä frequency, N, is a measure of the oscillations.

$$N = \left(\frac{-g}{\rho_0} \frac{d\rho}{dz} \right)^{\frac{1}{2}}, \tag{1.2}$$

where g is the acceleration due to gravity, ρ_0 is the average density of the fluid, $\frac{d\rho}{dz}$ is the stratification density gradient (< 0 for stable). For a particle of characteristic length a, moving with speed V in a stratified fluid with kinematic viscosity ν and thermal diffusivity κ, we have

$$Re = \frac{aV}{\nu}, \tag{1.3}$$

$$Fr = \frac{V}{aN}, \tag{1.4}$$

$$Pr = \frac{\nu}{\kappa}. \tag{1.5}$$

Using Re, Fr and Pr, the flow dynamics can be divided into different regimes discussed in [1, 8], and summarized in the next two sections.

1.3 Wake of a settling sphere in a linearly stratified fluid

The flow past a sphere in a stratified fluid (finite Fr) is inherently different from the homogeneous case ($Fr = \infty$). This is because stratification leads to a length scale l_s which is of significance in addition to the length scales in a homogeneous fluid. This length scale l_s is a function of Re, Fr and Pr. The additional forces introduced by stratification alter the vertical motion of the fluid at this length scale l_s and lead to different flow regimes. Ardekani & Stoker [12] showed that in the absence of inertia ($Re = 0$), the classical Stokeslet solution is not sufficient to describe the flow physics in a stratified fluid and introduced a Stratlet formulation to solve for the flow structure. The Stratlet captures the effect of the baroclinic torque in the fundamental solution and introduces toroidal eddies. These eddies are centered along with the sphere and their length scale l_s is $(\frac{\nu\kappa}{N^2})^{\frac{1}{4}}$. The toroidal eddies continue to exist for a finite Re (0.05), irrespective of the Fr. The drift volume is high at this low Re due to viscous effects, which leads to large deflections of the isopycnals. However, at this Re, for strong stratification ($Fr \leq 1$) and large Pr (700), the baroclinic torque acts on the volume of light fluid dragged by the sphere and results in a structure of positive upward velocity behind it. This is a consequence of conversion of positive radial gradient in density in the wake of the sphere into positive vorticity. The structure thus leads to an asymmetric velocity field about the horizontal axis of the sphere. As Re is increased, the thickness of the dragged fluid column becomes smaller and the vertical velocity in the wake of the sphere increases. When Re reaches a value of 100, in a strongly stratified medium ($Fr \leq 1$), a thin upward jet dominates the structure of the wake (Figure 1.1 wake pattern 'B'). At the centerline of this jet, the fluid speed is several times larger than that of sphere itself [2, 11, 13–15]. In the far-field, for $Fr \leq 1$ and $Re \approx 100$, internal lee waves define the flow structure [16]. For a given

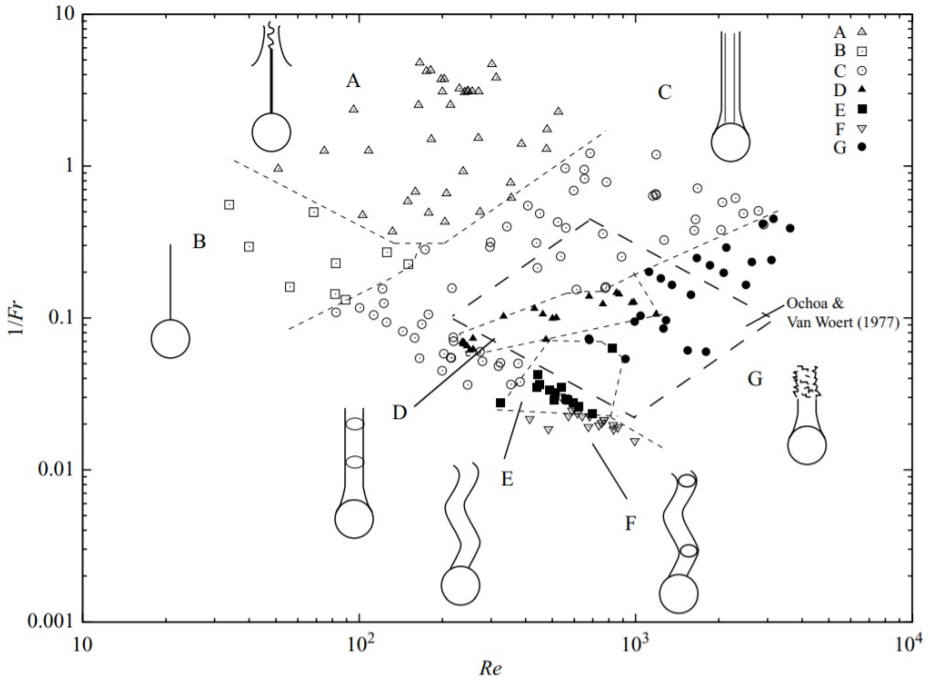

Fig. 1.1. Wake patterns of a sphere settling in a stratified fluid. Figure adapted from [17] with permission from Cambridge University Press

Re and Fr, increasing the Pr has a thinning effect on the jet and also increases the upward velocity of the jet [14].

At very low values of Fr (≈ 0.3) and moderate Re (≈ 200), in addition to the jet observed for $Fr \leq 1$, a bell shape structure is observed downstream of the sphere in both numerics and experiments (Figure 1.1 pattern 'A'). [13, 15, 17, 18]. The distance between the rear-stagnation point and the start of the bell shape is a function of the velocity of the sphere and N alone. In addition, the thickness of the jet in pattern 'A', 'B' in Figure 1.1 is also independent of Re and Fr and is controlled by N. The independence of these structures from the size of the sphere and viscosity of the fluid suggests that they are caused and controlled by internal lee waves in the far field. This observation in experiments by [17] supports the claim in the numerical work of [13] that the vertical distance separating lines of same phase in the vicinity of the sphere is under-predicted by the linear internal wave theory proposed in [16]. Pattern 'C'

in Figure 1.1 shows a thicker jet in the wake of the sphere. This jet is different from the one observed in pattern 'A'. In pattern 'C', high Re ($\approx$ 2000), leads to smaller density gradients and weaker diffusion. As a result, the sphere continuously deforms isopycnals dragging most of light fluid along in the jet. In pattern 'A', as the sphere descends, the isopycnals are deformed but stronger diffusion restores the light fluid to its original height earlier than pattern 'C'. In other word, in pattern 'A', the sphere cuts through the isopycnals as diffusion restores the light fluid being dragged.

A broad jet is also observed for weak stratification ($Fr = 7.2$) and moderate Re (= 678), pattern 'D'. This jet is however unsteady and generates knots periodically with the generation frequency directly proportional to Fr. Increasing the Fr ($\approx$ 34.7, Re = 567) introduces meandering to the shape of the jet while the knots are not present, pattern 'E'. Before the jet becomes fully turbulent at very high Re (2467, Fr =4.7) as in pattern 'G', weakening the stratification results in a spiralling jet periodically generating knots as observed in pattern 'F' ($Re = 589$, $Fr = 40.6$) [17].

1.4 Drag enhancement by stratification

As a consequence of the added toroidal vortex and entrained light fluid in the wake of a moving sphere, the drag force experienced by it is modified, compared to the homogeneous case. Torres *et al.* [13] investigated the effect of Fr on the drag experienced by a sphere settling at $Re = 200$ in a linearly stratified fluid through numerical simulations. As Fr decreased beyond 20, the value below which the axisymmetric wake in a homogeneous environment vanishes and the upward jet appears, an increase in both pressure and viscous drag was observed. Pressure contours accumulated behind the sphere as Fr decreased resulting in large reduction of pressure at the rear stagnation point. This low pressure region right behind the sphere is the reason for increased pressure drag. The low pressure region not only increased the pressure drag but also increased the vertical velocity of the fluid in the wake of the sphere. As a result, the velocity boundary layer around the sphere decreased,

increasing the viscous shear stress and thus the viscous drag. It is also important to note that the increase in viscous drag due to faster moving fluid around the sphere was larger than the increase in pressure drag for a given $Fr \leq 20$. Yick *et al.* [19] studied the effect of both Re and Fr at low Re and found that the drag enhancement correlated better with viscous Richardson number Ri (the ratio of Re and Fr^2) as suggested by the theoretical work of Zvirin & Chadwick [20]. The range of Re covered by Yick *et al.* was 0.05 to 2.1 across experiments and numerics. This complemented earlier works at high Re. The dependency of the normalized drag coefficient (ratio of drag coefficient in a stratified fluid and the one at the same Re in a homogeneous fluid) was found to be of the form $1 + \alpha_d Ri^\beta$ with α_d and β varying by 2% and 33% respectively in numerics from experiments. An increased pressure gradient due to large deflections of isopycnals at low Re and increased shear stresses due to generation of baroclinic torque caused by the deflected isopycnals enhanced the pressure and viscous drag, respectively. The third dimensionless parameter altering the flow structure, Pr, also modifies the drag experienced by the settling sphere. The observations reported above correspond to a Pr value of 700 (for salt stratification in water). As decreasing Pr weakens the characteristic downstream vortex at low Re and broadens the jet at $Re > 1$ [14], the normalized drag coefficient decreases with Pr. The decomposition of the enhanced drag force into a buoyancy induced drag (due to drift and entrainment of light fluid) and vorticity induced drag (due to changes in the flow structure) revealed that the latter has a larger effect for density stratified fluids ($Pr = 700$). This leads to a conclusion that the baroclinic torque generates more extra drag than the drift volume [11].

An increased drag force has direct implications on the steady-state settling velocity of the spheres. The path taken by the sphere to reach the steady state velocity is also different in a stratified fluid. At $Pr = 700$, $Re = O(10^2)$ based on the Fr, the settling velocity of sphere can either monotonically decelerate, oscillate and decelerate or levitate. The frequency of oscillation is independent of the Fr and scales with N. Levitation is observed when the stratification is strong and the difference between

particle and local isopycnal density is small. An increase in Re increases the distance taken by the particle to reach its steady state velocity and also increases the Fr up-to which levitation is observed [2].

1.5 Effect of stratification on particle-particle interactions

When a suspension of particles settles in a stratified fluid, apart from the effects of stratification, particle-particle interactions and hydrodynamics also affect the settling and flow. Even in a simple situation of a pair of particles, the particle-particle interactions are greatly modified in the presence of stratification. If the particles initially start next to each other (perpendicular to the stratification), the particles do not repel each other and reach a distance of separation. Instead, they are attracted to each other with their final separation distance decreasing with the stratification strength (decreasing Fr) and increasing Pr. The mechanism behind this attraction is the interaction between the downstream jets behind the spheres, which is absent in homogeneous fluids. The downstream jets interact and form a stronger jet pushing the fluid upward. Increasing Pr and decreasing Fr have a thinning effect on the jets of individual spheres, the jet in between the spheres also thins out, pulling the spheres together. The particles are not attracted to each other as soon as they are released. Because of larger initial effect, the particles are initially repelled as in a homogeneous fluid. After reaching a certain depth, once the downstream jets have developed, the effect of attractive forces due to stratification kicks in. As it can be inferred, the attraction of the spheres to each other is counteracted by inertia. In other words, for a fixed Fr and Pr, if the Re is increased, the particles take longer to come in contact with each other. In a tandem configuration, where the spheres are released one below the other in the direction of stratification, the spheres undergo *drafting, kissing and tumbling* (DKT) in a homogeneous fluid. The sphere downstream is pulled into the wake of the leading sphere (*drafting*), the spheres come in contact with each other (*kissing*) and they interchange their positions with the leading sphere now trailing

(*tumbling*). In the presence of stratification, the interaction is altered. In weak stratification, the extent of *tumbling* is reduced thus altering the particle positioning and dynamics after *kissing*, the duration of which is also observed to increase. For moderate stratification ($Fr \leq 12$), DKT transitions to *drafting, kissing and separation* where after *kissing* the particles maintain their positions (leading and trailing particle) and separate from each other in the direction of the stratification. On further decreasing the Fr, the *kissing* stage is eliminated owing to strong buoyancy forces (because of strong stratification). As a result, the trailing particle reverses direction of its motion prior to touching the leading particle [21].

The time-average mean particle velocity, U_p, of a suspension settling in a stratified fluid has been observed to reduce in both experiments and numerics [22, 23].The difference between U_p and the volume averaged fluid velocity is called slip velocity. For a single particle, the drag law proposed in [19] can be used to calculate the ratio between slip velocity of a settling sphere in a stratified fluid to that in homogeneous fluids. The ratio is of the form $1 - 10.3Fr^{-1.7}$. Doostmohammadi & Ardekani [23] perform direct numerical simulations of a suspension of 8 spheres settling in a linear stratified fluid. The slip velocity for the suspension in a linearly stratified fluid is found to be $1 - 61.1Fr^{-2.07}$ times the slip velocity in homogeneous fluid. It can be concluded from these two empirical relations that stratification has a larger effect on reducing the slip velocity for a suspension than for an individual particle. This reduction in slip velocity in suspensions, leads to aggregation and cluster formation. The radial (angular) pair correlation function, $g(r)$ ($g(\theta)$), is the probability of finding a second particle at a distance r (angle θ) from the center of a particle of interest. A peak was observed in $g(r)$ at $r = 1.5d$ and $g(r)$ diminished beyond $r = 5d$ indicating that the clusters are formed at short distances. Peaks were observed for $g(\theta)$ at $\theta = \frac{\pi}{2}$ from the vertical axis indicating that the particles are mainly aligned in the horizontal direction within the cluster. For stronger stratification, unstable vertical alignment of the particles was also observed through unstable peaks at $\theta = 0$ and $\theta = \pi$. The horizontal clustering of particles is a consequence of the attraction experienced by

two particles released next to each other side-wise while the unstable nature of the vertical clustering is a consequence of the *drafting, kissing and separation* that a pair of particles would experience when released in tandem [1, 23].

1.6 Energy transport and mixing

In a stratified fluid, the total energy of the system can be divided into background or reference state potential energy and available potential energy. Background potential energy is defined as the minimum amount of energy in the system attained by adiabatic rearrangement of fluid in the system to a state of minimum potential energy. Available potential energy is the amount of energy spent in the adiabatic rearrangement of the system [24]. As a particle or a group of particles moves across a stratified fluid, the deflection of isopycnals modifies the background potential energy of the system. As the displaced fluid relaxes to its initial depth due to buoyancy, it stretches the material interfaces over which diffusion occurs by altering local perturbations of the density gradient. This leads to stirring of the system and enhances mixing. By understanding and quantifying these energy budgets and their modification due to particle settling, the questions unanswered in the fore-mentioned applications can be addressed.

Blanchette [25] developed a phase diagram relating the extent of mixing caused by a suspension of particles settling in temperature stratified air (low Pr) to volume fraction. The diagram was based on qualitative classification of the temperature map after time $t = 5/N$. Important takeaways from the study included evidence for significant contributions to mixing of air around volcanoes and forest fires by settling ash particles and water bodies near river beds by swarms of particles typically found. Wang & Ardekani [4] quantified mixing induced by active suspensions swimmers in a density stratified fluid with background turbulence. By evaluating mixing efficiency, diapycnal eddy diffusivity and COX number, the interaction between the squirmers

and background turbulence and the viscous dissipation of the swimming motions was found to contribute to local mixing.

1.7 Scope of this thesis

The present work focuses on experimentally quantifying the mixing induced by settling particles. Solid spheres and cylinders of different densities are used and experiments are performed for different stratification gradients to cover a range of Re and Fr. Experiments are performed for individual particles and for a groups of particles to understand collective effects. The double-tank method is used to setup a linear stratification [26]. The salt water used is marked using a dye. Hence stratification in both dye and salt concentration is achieved. This serves as a tool to track density throughout the experiment.

This thesis is organized in the following order. Chapter 2 introduces the experimental setup, explains the measurement techniques used to extract raw data, the data processing algorithms used to extract the variables of interest from raw data and the uncertainty analysis. Chapter 3 presents the results of the experiments and explains the physical reasoning behind the events and trends observed.

2. EXPERIMENTAL METHODS

The experiments were performed at Institut de Mécanique des Fluides de Toulouse (IMFT), France. A schematic of the experimental setup is shown in 2.1. The goal of the study was to investigate 2D characteristics of particles settling in a confined environment. A 0.75 m high glass tank with a rectangular section (0.36 m x 0.042 m) is used. The tank has an opening at the bottom to feed the stratification. A double-tank method is used to generate the stratification. Two tanks with a capacity of 6 litres each are interconnected at their bases using a horizontal pipe and a valve. The first tank is filled with heavy water with homogeneously dissolved sodium chloride and a dye. The second tank is filled with undyed fresh water to the same level as the first tank. Fluid from the second tank is fed into the experimental tank using a peristaltic pump keeping the valve between the tanks open and continuously stirring the second tank using a mechanical stirrer. The feeding process is done at low flow rates to minimize mixing at the inlet of the experimental tank. Stratification in the density of fluid and concentration of dye is achieved. A dropping system (Figure 2.2) with a spring attached gate is designed and used to release the objects. The dropping system helps releasing multiple objects at the same instant in time in a given experiment and ensures the object(s) to be released from the same height in different experiments. The center plates of the dropping system are pulled away from each other to open the gate and release the objects. The gate is made using a corrosion resistant sheet of steel for longevity and to minimize contamination of the tank. Small holes are drilled in the bent portion of the gate to allow any fluid pushed during the opening of the gate to flow back horizontally. The dropping system is designed and mounted to the tank such that the objects are immersed below the free surface of the fluid and any surface bubbles on the objects are eliminated. Opening and closing of the gate is done slowly to minimize any mixing caused by the release process. Objects

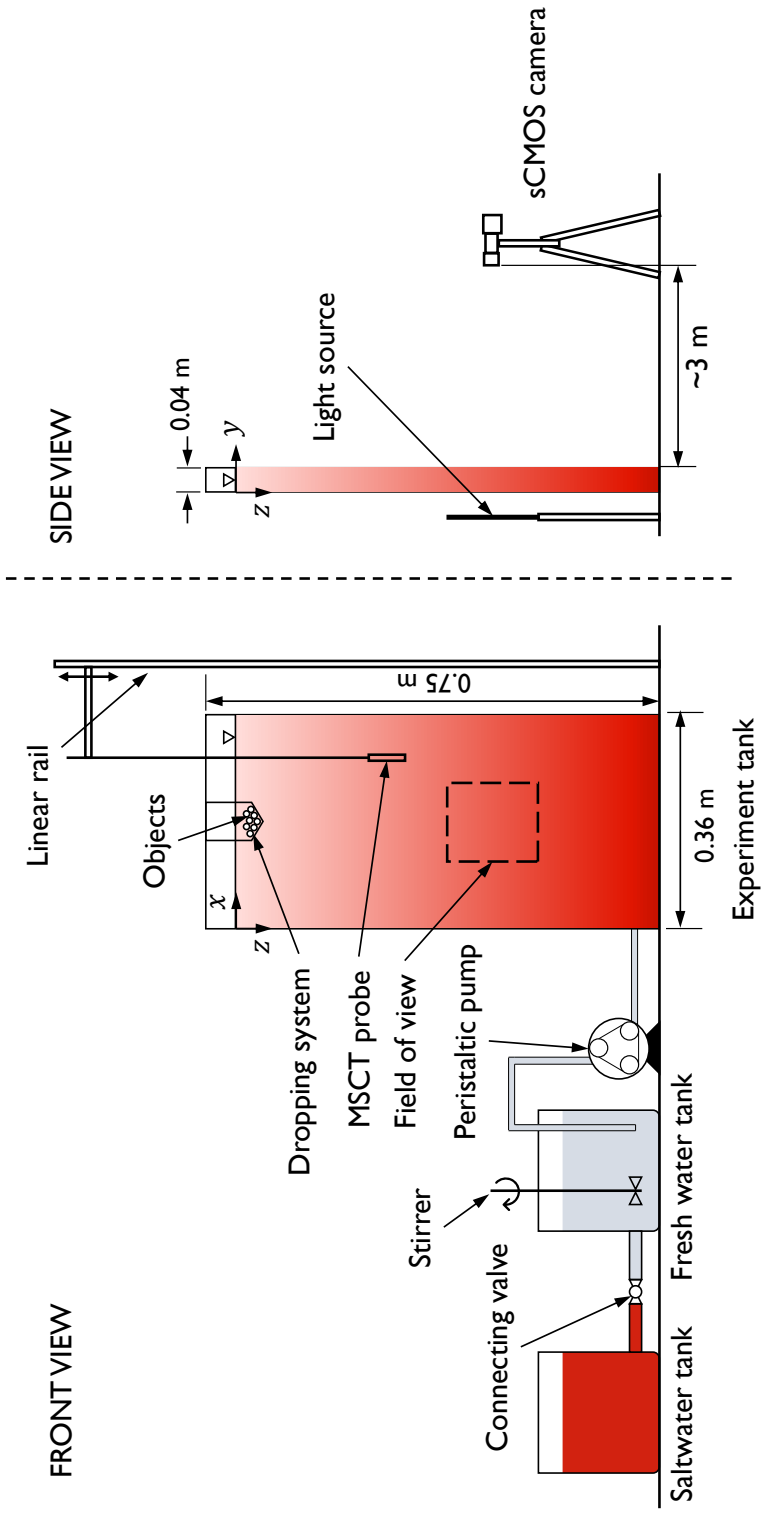

Fig. 2.1. Schematic diagram of the experimental setup

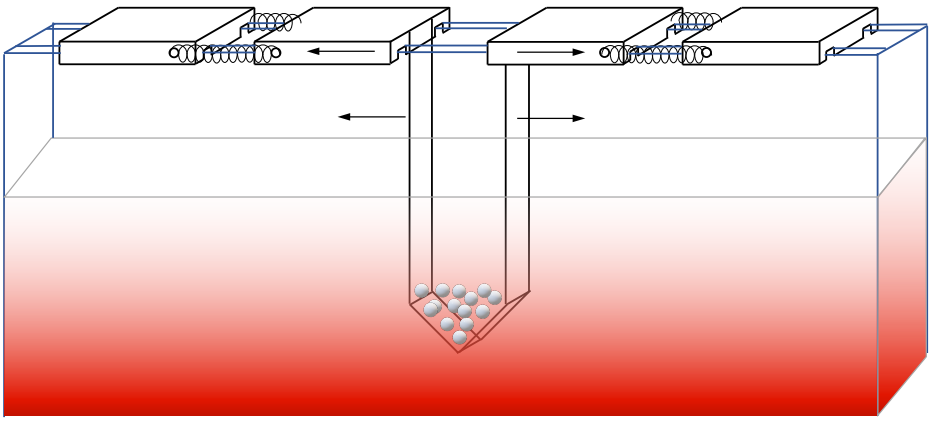

Fig. 2.2. Dropping system used to release objects

of two different geometries, *viz.* spheres and cylinders, are used. Polished Airsoft pellets with a 6 mm diameter are used for the spheres. The standard deviation of the diameter of the high precision, ultra smooth spheres is $\pm 0.01mm$. Spheres of four different densities are used to achieve different Re for a given density stratification. The goal of the study is to investigate 2D characteristics of particle settling, thus, the length of cylinders is chosen such that they remained aligned with y coordinate during the entire experiment. Description of the objects used in settling experiments are tabulated in Table 2.1. Once stratification is fed into the experimental tank, experiments are performed for both single and multiple objects being released. For experiments involving multiple spheres, the number of spheres is chosen such that

Table 2.1.
Size and density of objects used in settling experiments

Object	**Diameter, a (mm)**	**Length, L (mm)**	**Density, ρ_p (kg/m^3)**
Sphere	6	N/A	1037, 1405, 1805, 2091
Cylinder	10	41.1	1322, 1370
Cylinder	20	39.6	1335

the total volume of the spheres is equal to the volume of one/two 10 mm diameter cylinders. A significant delay between experiments ensures disturbances due the preceding settling experiment have dissipated. This allows using the same density stratification for multiple experiments. The delay between experiments is at least 5 min for individual spheres, at least 15 min for suspensions of spheres, single and multiple cylinder experiments.

2.1 Flow visualization

The dye dissolved in the heaviest fluid is used as a tool to quantify density. A digital camera along with a powerful back-light is used to capture the settling events. The camera and back-light are placed as shown in Figure 2.1. The camera used has a black and white scientific complementary metaloxidesemiconductor (sCMOS) sensor

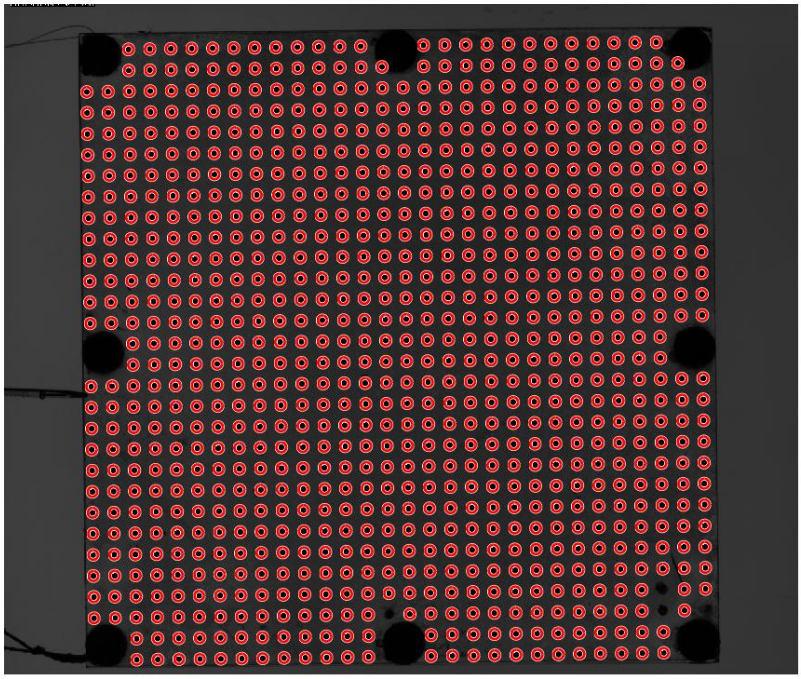

Fig. 2.3. Length calibration grid used with circles identified

with 2560 x 2160 pixels with each pixel saving 16 bits of data. The camera is placed approximately 3 m from the tank to minimize parallax error. All recordings are done with an exposure time of 2 ms at a frame rate of 49.997 Hz. A plumb line is recorded and the camera tripod adjusted such that the longer edge of sensor is aligned with gravity. The intensity of light that reaches the sensor of the camera is an average of the events along the thickness of the tank. This means, the measurements performed are 2D observations of the events in the tank. The field of view of the camera is a 18.88 cm x 15.88 cm window, at least 30 cm below the point of release of the objects and 15 cm above the base of the tank. This translates to 50 diameters and 25 diameters respectively for the spheres and 30 (15) diameters and 15 (7.5) diameters for the 1 (2) cm cylinders A teleconverter is used to double the focal length of the lens and the focus is adjusted such that an object is in-focus both at the front and and rear face of the tank. In order to quantify the length of each pixel, a 30 x 30 grid of 2 mm diameter circles is placed inside the experiment tank while filled with water. An average of 256 images is captured using the camera. By using the function *imfindcircles* in MATLAB, the diameter of each circle in the grid is measured in pixel units. The average pixel diameter of all the circles is used to convert from pixels to length units. The length of a pixel varies by 0.2 μm over the depth of the tank, the

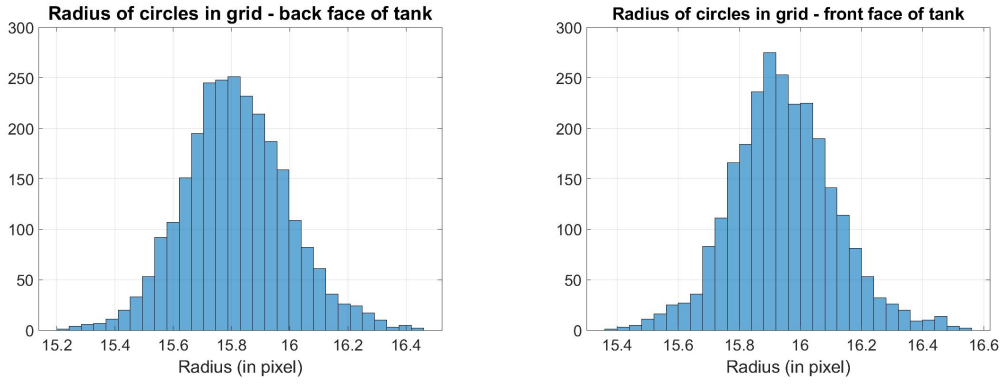

(a) Grid at back face of tank

(b) Grid at front face of tank

Fig. 2.4. Histogram of radius of the circles identified

average is used as the pixel-length scale for all calculations. A sample image used to perform this operation is shown in Figure 2.3 and the distribution of radii calculated is shown in Figure 2.4.

A calibration is performed to quantify density from the images captured. In order to do so, the fresh water and dyed heavy water used to generate the stratification are prepared in large quantities. For the purpose of calibration, at least five homogeneous mixtures of fresh water and dyed water in different ratios are prepared. The density of each mixture prepared is measured using an Anton Paar density meter. Images of the homogeneous mixtures of different densities ranging from fresh water to the heaviest water are captured using the camera back-light setup. Using this set of images, Beer Lambert's law is used to correlate the intensity of light sensed by the camera to the density of the fluid (Equation 2.1). For the concentration of dye used, a quadratic fit gives a good correlation.

$$\ln\left(\frac{I}{I_0}\right) = A(\rho - \rho_0)^2 + B(\rho - \rho_0) + C \tag{2.1}$$

where ρ is the unknown density of a pixel of interest, ρ^0 is the density of fresh water used during calibration, I is the intensity of pixel of interest, I_0 is the intensity of the pixel of interest during calibration with fresh water and A, B, C are coefficients

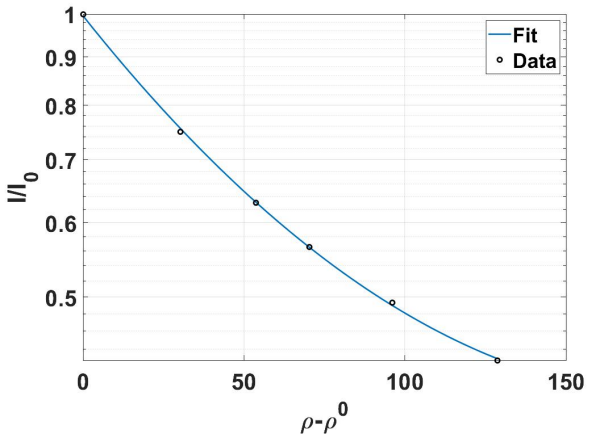

Fig. 2.5. Quadratic fit used to calibrate density as a function of intensity

of the quadratic fit determined by calibration. An example of this calibration law is shown in Figure 2.5.

2.2 Temperature-density probe

Apart from using the dye to measure density, a MicroScale Conductivity Temperature (MSCT) probe is used (Figure 2.6). The probe consists of a rod mounted with two electrodes at its bottom tip. One of the electrodes is a thermocouple and the other electrode provides a voltage output based on the electrical conductivity of the surrounding medium. As the electrical conductivity of water is directly proportional to the density of ions present in it, the output of this electrode can be used as a measure of density. The voltage gain of the conductivity electrode is adjusted to get reliable output for the entire range of densities to be measured in the experimental tank. By preparing solutions of known density in the range of interest, a calibration curve is generated for voltage and density and voltage and temperature. The probe is mounted to a motor actuated linear rail such that the probe can move inside the experimental tank and can measure density as a function of depth (Figure 2.1). The position of the linear rail can be measured continuously with a least count of 10^{-6}

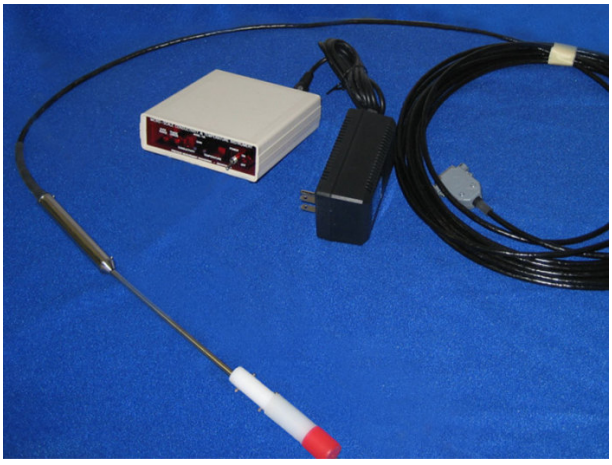

Fig. 2.6. MicroScale Conductivity Temperature probe

mm. By using an electronic circuit, synchronized recording of the position of the rail and electrode voltages is carried out. From the voltage output, using the voltage calibrations, the temperature and density of the fluid is determined as a function of depth. This density profile is used to estimate the amount of mixing induced.

2.3 Data processing

Rewriting Equation 2.1 in terms of density, we have

$$\rho = \rho^0 + \left(\frac{-B \pm \sqrt{B^2 - 4A(C - \ln I + \ln I_0)}}{2A} \right) \tag{2.2}$$

Equation 2.2 is used to evaluate density from all images captured. The term in the exponential is the quadratic root of Equation 2.1. The smaller value of the two roots gives a physically acceptable value for density. Figure 2.7 shows the intensity as sensed by the camera with homogeneous undyed fresh water in the experiment tank. As it can be seen, the back-light used does not uniformly illuminate the field of view. To account for non-uniformity of the back-light, the calibration images are divided into overlapping grids and calibration coefficients are determined for each grid.

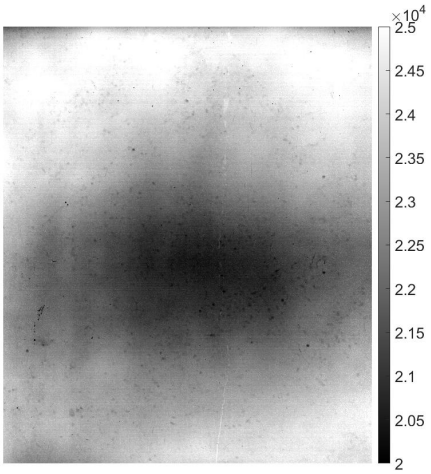

Fig. 2.7. Non-uniformity of the back-light

Figure 2.8 shows the spatial variation in the calibration coefficients A, B and C over the domain and the square of the residue for the quadratic calibration fit. Another observation from Figure 2.7 is that near the edges of the image, strong gradients in light intensity are present. In a strongly stratified fluid, disturbances by the settling objects will cause strong local density gradients. The gradients due to non-uniformity along with gradients in intensity due to change in local density optically limit the reliability of measurements. In order to account for this optical limit, density data near the edges of the image is discarded. The width of the discarded region is 5 calibration window lengths and it is marked in Figure 2.8. Figure 2.9 shows the spatial variation in calibration coefficients for another set of experiments with a

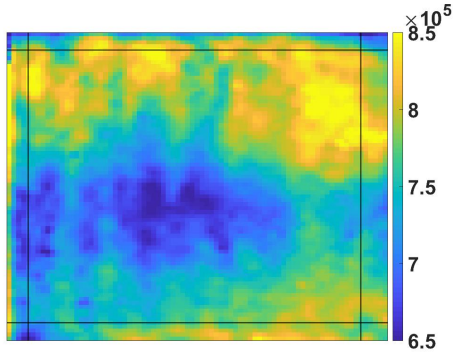

(a) Calibration coefficient A

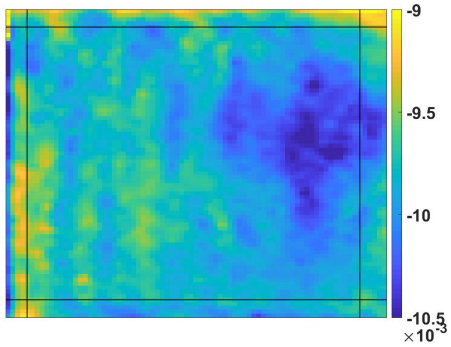

(b) Calibration coefficient B

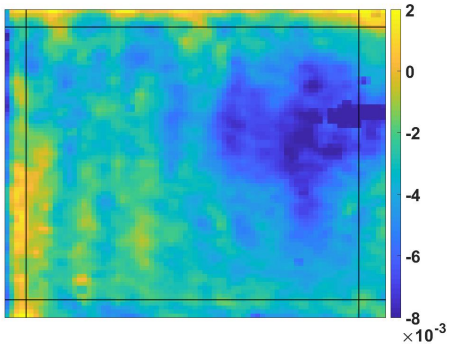

(c) Calibration coefficient C

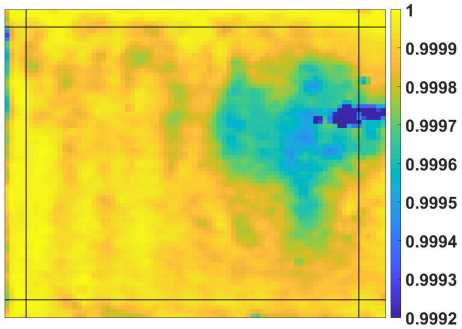

(d) R^2

Fig. 2.8. Spatial variation of calibration law

different stratification. The maps being similar to those in Figure 2.8 confirms that the spatial variation is indeed caused due to the non-uniformity of the back-light. When dividing the image into calibration windows, a 50% overlap in both x and z direction is used to eliminate discontinuity in data across grid boundaries. In regions where multiple calibration laws are valid due to overlap in the calibration windows, average of the density evaluated using all the valid laws is used. This process is illustrated in Figure 2.10. A sample image is taken and a simple division into calibration windows is considered. The size of all calibration windows in the figure is a quarter of the size of the image. The density at each pixel in regions numbered 1, 4, 13 and 16 is equal to the density evaluated using calibration laws I, III, VII and IX, respectively. In

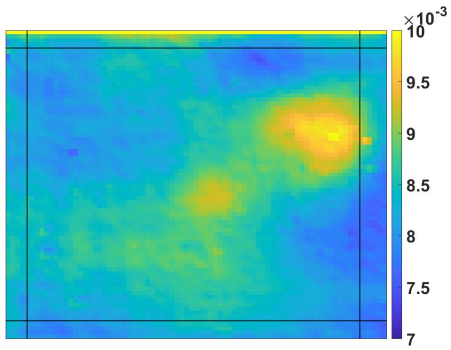

(a) Calibration coefficient A

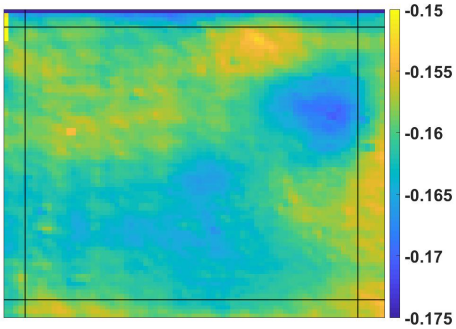

(b) Calibration coefficient B

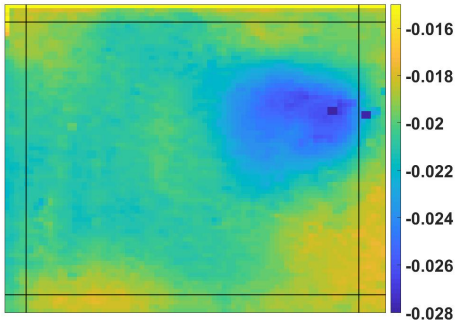

(c) Calibration coefficient C

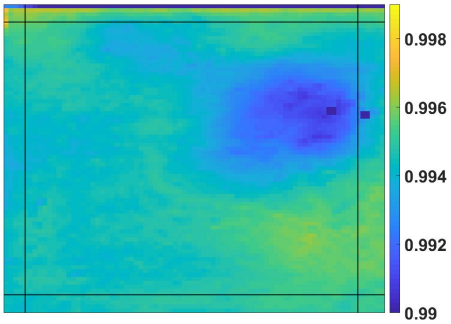

(d) R^2

Fig. 2.9. Spatial variation of calibration law - Calibration 2

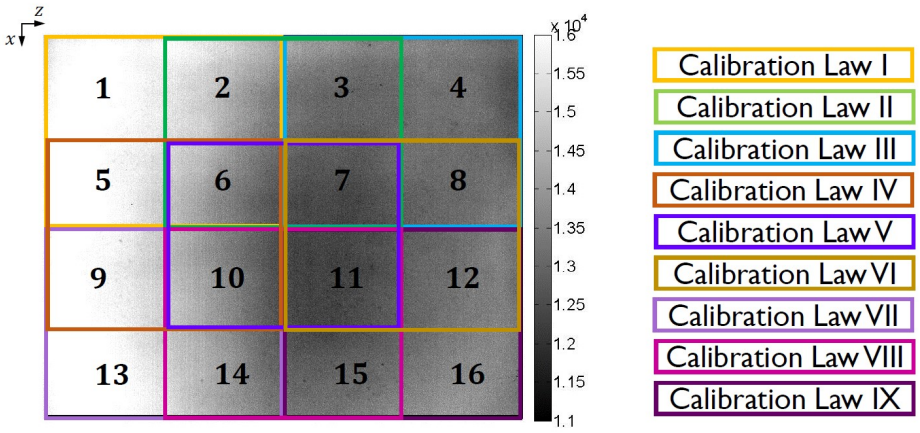

Fig. 2.10. Density evaluation with overlapping calibration windows

regions 2, 3, 5, 8, 9, 12, 14 and 15 the density at each pixel is equal to the average of density calculated using calibration laws (I,II), (II,III), (I,IV), (III,VI), (IV,VII), (VI,IX), (VII,VIII) and (VIII,IX). Finally, the average of density calculated using calibration laws (I,II,IV,V), (II,II,V,VI), (IV,V,VII,VIII) and (V,VI,VIII,IX) is used in regions 6, 7, 10 and 11, respectively.

2.4 Uncertainty analysis

The uncertainty in density calculations can be attributed to three sources, noise in the raw images captured by the camera, uncertainty in the density meter used to measure density during density-intensity calibration and the uncertainty associated with the coefficients determined by the quadratic fit. The density meter used to measure ρ_0 was a digital device with a least count of 0.1 kg/m^3, thus giving an absolute uncertainty $\Delta\rho_0 = 0.1kg/m^3$. All experiments were conducted in a dark environment with the back-light being the only source of illumination. To quantify the uncertainty due to camera noise, images were captured in the same dark environment as used during the experiments with the back-light turned OFF. As there is no other source of illumination, any value read by the sensor of the camera would be because

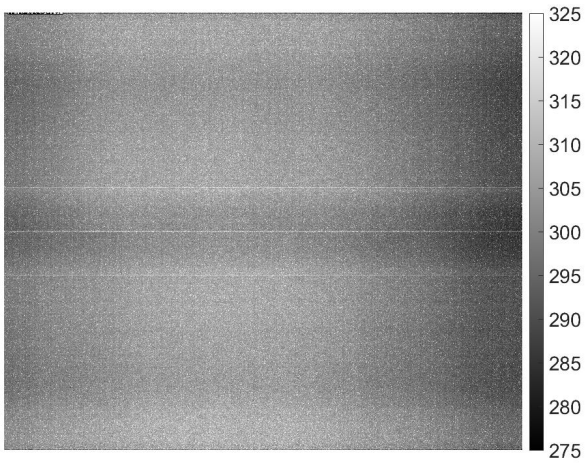

Fig. 2.11. Camera noise

of its own noise and other environmental noise (if any) present. Figure 2.11 is the average of 256 images taken with the back-light OFF. The maximum intensity in the image (I_{max}) is equal to 325.84. I_{max} is the absolute uncertainty associated with the intensity of any pixel, *i.e.,* $\Delta I = \Delta I_0 = 325.84$. When concentration of dye used is maximum, the pixel intensity sensed by the camera with the back-light ON would correspond to the minimum value of signal in any experiment. This value of pixel intensity was 8627.4 giving a maximum $\Delta I/I$ of 0.0377. MATLAB was used to do all data processing and analysis. The quadratic fit for the calibration laws was generated using the in-built function *polyfit*. Outputs of this function are the coefficients of the fit (A, B and C), the Vandermonde matrix from the least square fitting of the polynomial, degrees of freedom and norm of the residue. Using this data, the standard deviation in A, B and C is calculated.

In any given image, because of the non-uniformity in the back-light and because of the density stratification, I, and I_0 vary with x and z. A, B and C also vary spatially as a consequence of spatially varying calibration laws. Hence, uncertainty in density is a function of x and z. This uncertainty is evaluated and used to separate noise from data while evaluating density disturbance caused by settling objects and for calculat-

ing parameters derived from density. Further details on uncertainty evaluation can be found in Appendix A. A sample image, the calculated density and its uncertainty are shown in Figure 2.12.

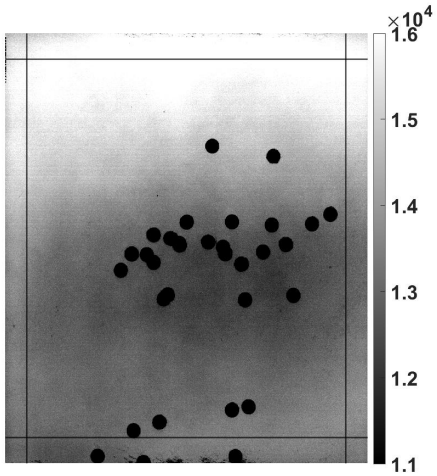

(a) Raw image

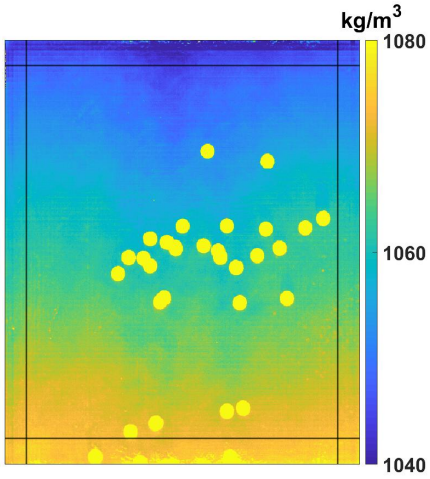

(b) Density field

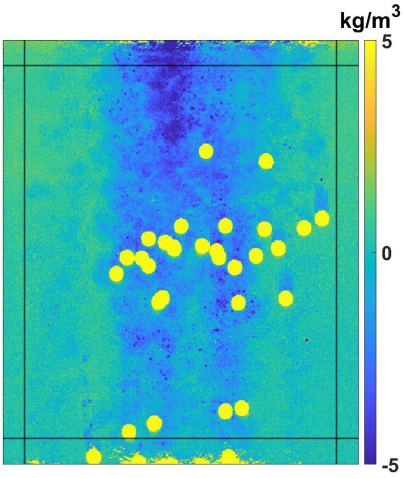

(c) Density change

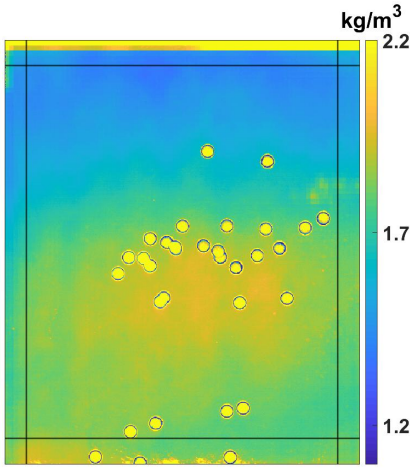

(d) Absolute uncertainty $\Delta\rho$

Fig. 2.12. Density field and associated uncertainty

3. RESULTS AND DISCUSSION

Experiments were performed for two different stratification strengths. For each stratification strength, multiple sets of experiments were performed. A particle(s) was released using the dropping system (Figure 2.2) and the events were recorded. By allowing sufficient delay, the next experiment was performed without changing the stratification. For each experiment, at least 25 images were recorded before the particle(s) entered the field of view to characterize the initial density field in the tank. The initial density field was averaged along the x direction to get the initial $\rho(z)$ for the image. The slope $d\rho/dz$ and mean ρ_0 were used to calculate the Brunt-Väisälä frequency, N from Equation 1.2. The initial value of N before any experiment performed was 0.37 s^{-1} and 1.22 s^{-1} for the two stratification strengths. The camera recordings are 2D observations and the spheres and cylinders are used in experiments. The cylinders are released such that their axis is aligned with the y direction. As a result, all particles were captured as circles in the images recorded. The images are processed using the function *imfindcircles* in MATLAB and the (x, z) location of the centers of each particle is identified. A predefined intensity threshold was used to separate the solid particles from the fluid in the image and by using the known length of a pixel evaluated in Section 2.1, bounds were provided for the size of the circles. Using the (x, z) location of each of the particle's center, tracking features of the open-source software *prana* were used to reconstruct the trajectory of the particle and evaluate its speed. Using the time-averaged value of the speed, the Re and Fr for the experiments are calculated (Equation 1.3, 1.4). Figure 3.1 shows the parameter space for the study. The points in the figure correspond to the values of Re and Fr based on the experiments with a single particle. The experiments with one released sphere were repeated 5 times and those corresponding to a cylinder were repeated thrice and the average Re and Fr are shown.

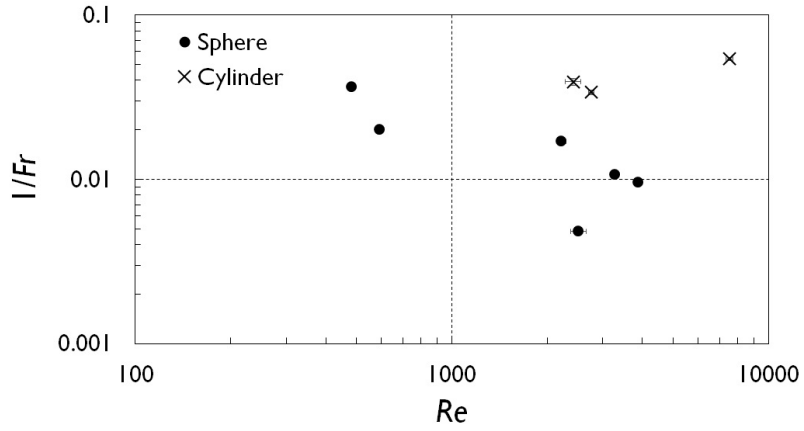

Fig. 3.1. Experiment parameter space

3.1 Particle velocity

The density of the fluid increases with depth in the experiment tank. As a result, the buoyancy force causing the particle to settle decreases with depth. Thus, the particle continuously decelerates as it settles. The ratio between the velocity with which a sphere enters the field of view and the velocity of the particle at a depth z is denoted by U_r. Figure 3.2 shows the evolution of U_r as the particle settles through the image. As the velocity of the spheres decreases linearly with z, it can be assumed

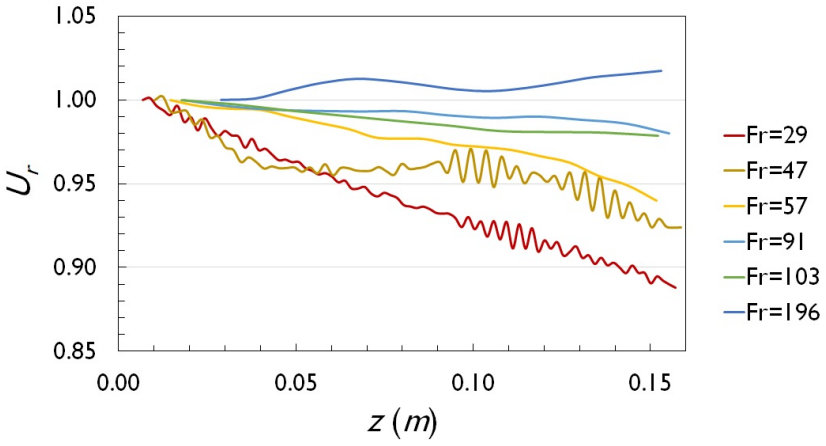

Fig. 3.2. Velocity reduction of a single sphere

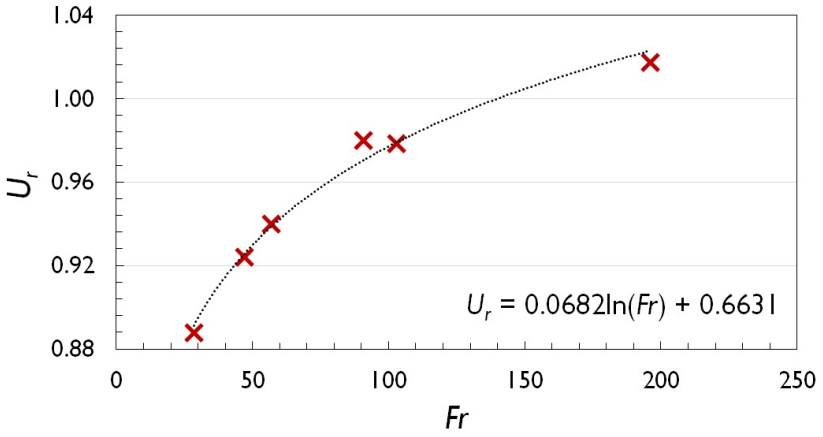

Fig. 3.3. Velocity reduction of a single sphere

that the particle reached quasi-steady state when it entered the field of view. As Fr decreases, the relative strength of buoyancy over inertia increases. In Figure 3.3, the ratio of the velocity of the particle at the exit and entrance of the field of view is plotted against Fr. U_r is found to be a logarithmic function of Fr given by $0.0682 \ln Fr + 0.6631$ $(29 \leq Fr \leq 196)$

When groups of particles are released, the time-average mean particle velocity decreases. Figure 3.4 shows the ratio of the time-average mean particle velocity of N_p

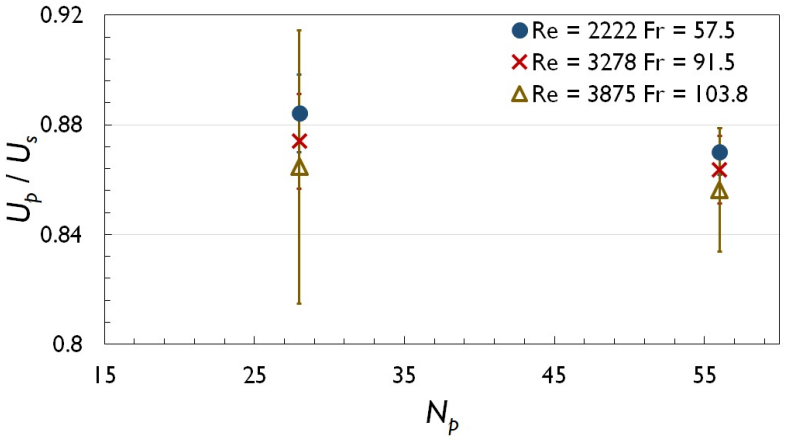

Fig. 3.4. Ratio of time-average mean particle velocity

number of spheres (U_p) to the velocity of a single sphere (U_s) settling in the tank with same initial N. The values plotted are an average of three repetitions of the experiment. It is observed that as N_p increased, U_p decreased in all the experiments. This reduction in U_p with increasing number of particles is consistent with the observations in [22, 23].

3.2 Density perturbations

3.2.1 Single particle

As it is seen in the previous section, stratification affects the transport of particles. The particles also affect the stratification. The particles drag volume of light fluid in their wake, deflect the isopycnals and perturb the density field. Figures 3.3 and 3.4 represent the maps of the disturbance in density field caused by a single sphere and a single cylinder, respectively. The maps are contour plots of the difference between the instantaneous density field and the initial density field. For the spheres, three distinct patterns are observed. In Figure 3.5(a), a jet of light fluid appears to be dragged by the sphere in its wake as it settles. The jet has a spiral nature, similar to pattern 'E' in [17] (Figure 1.1) for $Re = 491$ and $Fr = 31$. In Figure 3.5(b), another spiralling jet is observed with knots being generated in the jet. This transition from a stable jet to a jet with knots happens as the Fr increases and the effect of stratification is reduced. A similar observation is made in [17] for Re $O(100)$ as the wake pattern changes from 'E' to 'F' in Figure 1.1.

The Re in Figures 3.5(c) to 3.5(f) is $O(1000)$ and Fr increases from 59 to 196. The wake is fully turbulent in all these cases with stratification having little to no effect on the nature of the pattern similar to 'G' in Fig. 1.1. This is because the buoyancy force is relatively weak when compared to inertia. In all the wake patterns for the sphere, there is a region just behind the sphere where the amount of density disturbance is large relative to other regions downstream. This is the signature of weak stratification where buoyancy forces are not large enough to restore the light

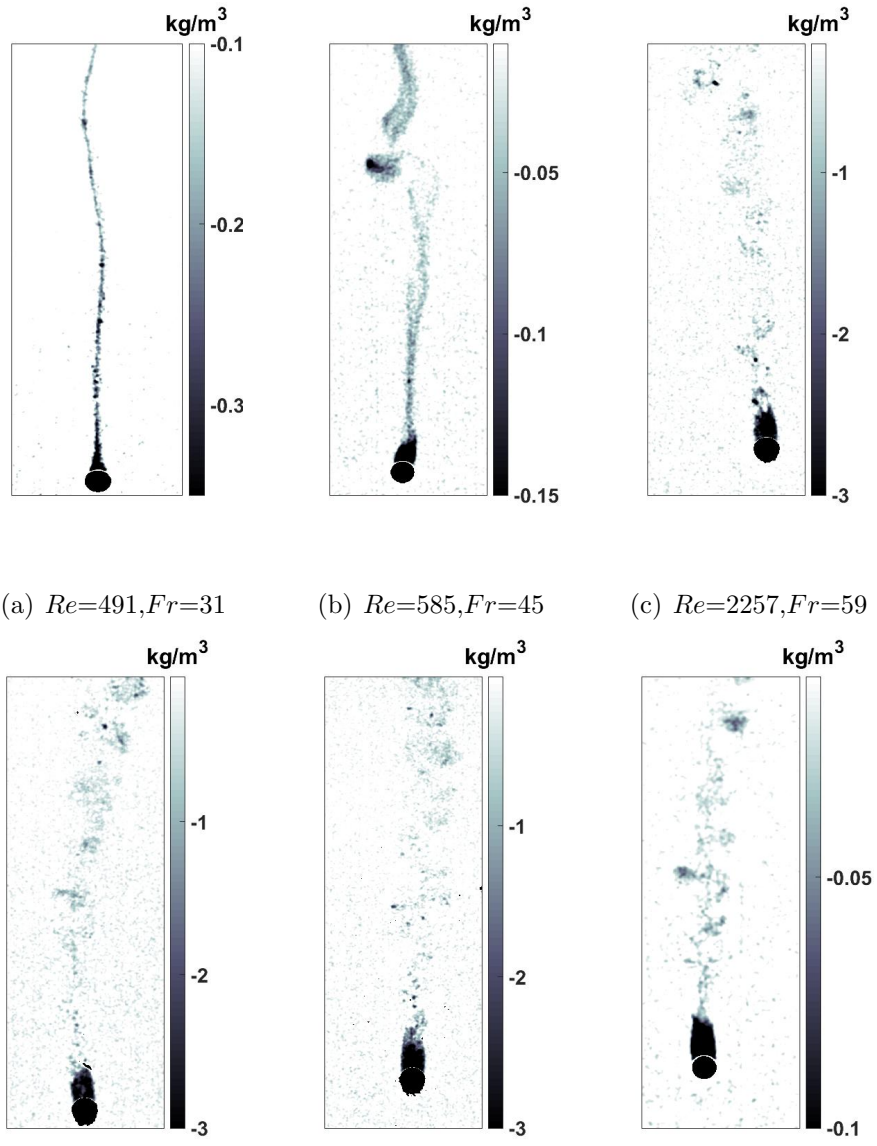

(a) Re=491,Fr=31 (b) Re=585,Fr=45 (c) Re=2257,Fr=59

(d) Re=3265,Fr=93 (e) Re=3907,Fr=104 (f) Re=2598,Fr=196

Fig. 3.5. Density disturbance field caused by a single settling sphere

fluid to its original height. The dominating inertial forces carry the light fluid in the wake of the sphere and isopycnals are continuously deformed by the settling particle.

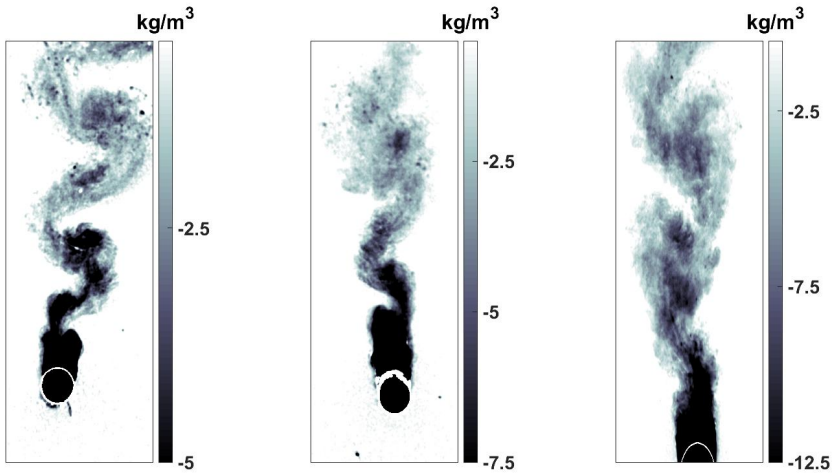

(a) Re=2332,Fr=24 (b) Re=2716,Fr=28 (c) Re=7524,Fr=18

Fig. 3.6. Density disturbance field caused by a single settling cylinder

Figure 3.6 shows the wake patterns observed for three different cylinders settling in a fluid with a similar initial density gradient. The dark blue region in the wake of the cylinder corresponds to the light fluid dragged by the cylinder in its wake as it settles. The cylinder sheds this light fluid in the form of vortices as it settles in the stratification. The size of the dark region behind the particle and the magnitude of the density disturbance increases with Re. This indicates that as the effect of inertia increases, the light fluid dragged by the cylinder is trapped in its wake to larger depths before being shed by the cylinder.

3.2.2 Suspension of particles

Figures 3.7 to 3.11 show the disturbance to the initial stratification caused by suspension of spheres. Each figure represents the disturbance caused by a suspension of spheres with the same ρ_p to the same initial stratification. The number of spheres, N_p, in the suspension is different in the top and bottom row. The left column of each figure shows the disturbance in the density field at the instant when all the spheres

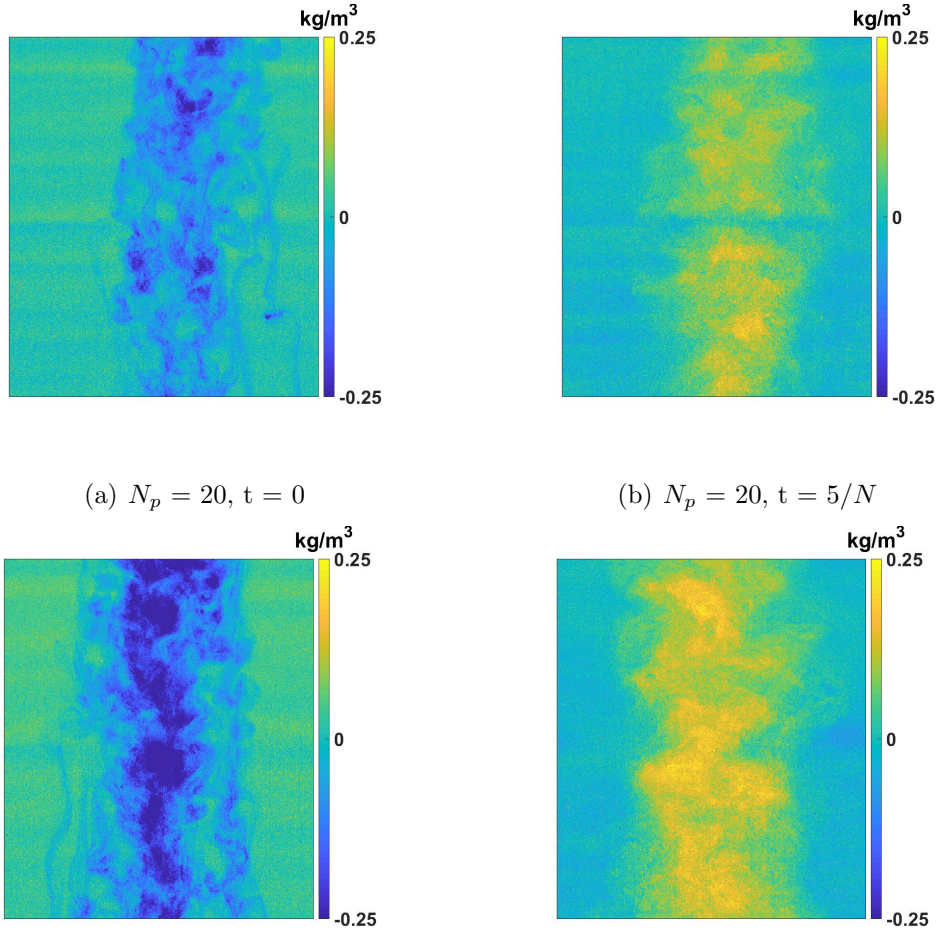

(a) $N_p = 20$, t = 0

(b) $N_p = 20$, t = $5/N$

(c) $N_p = 40$, t = 0

(d) $N_p = 40$, t = $5/N$

Fig. 3.7. Density disturbance field, N=0.37 s^{-1}, ρ_p=1037 kg/m^3

have just passed the field of view and the right column shows the disturbance after a time t = $5/N$.

The strength of the initial stratification was the same in Figures 3.7 and 3.8 with the density of the spheres being 1037 kg/m^3 and 1405 kg/m^3, respectively. The scale used in the colorbars is consistent in these figures to allow for a direct comparison of the disturbance caused. Figures 3.5(b) and 3.5(f) are the plots corresponding to the disturbance caused by the same sphere ($N_p = 1$). As N_p of spheres increases, the area of region with detectable disturbed density at $t = 0$ after the spheres have

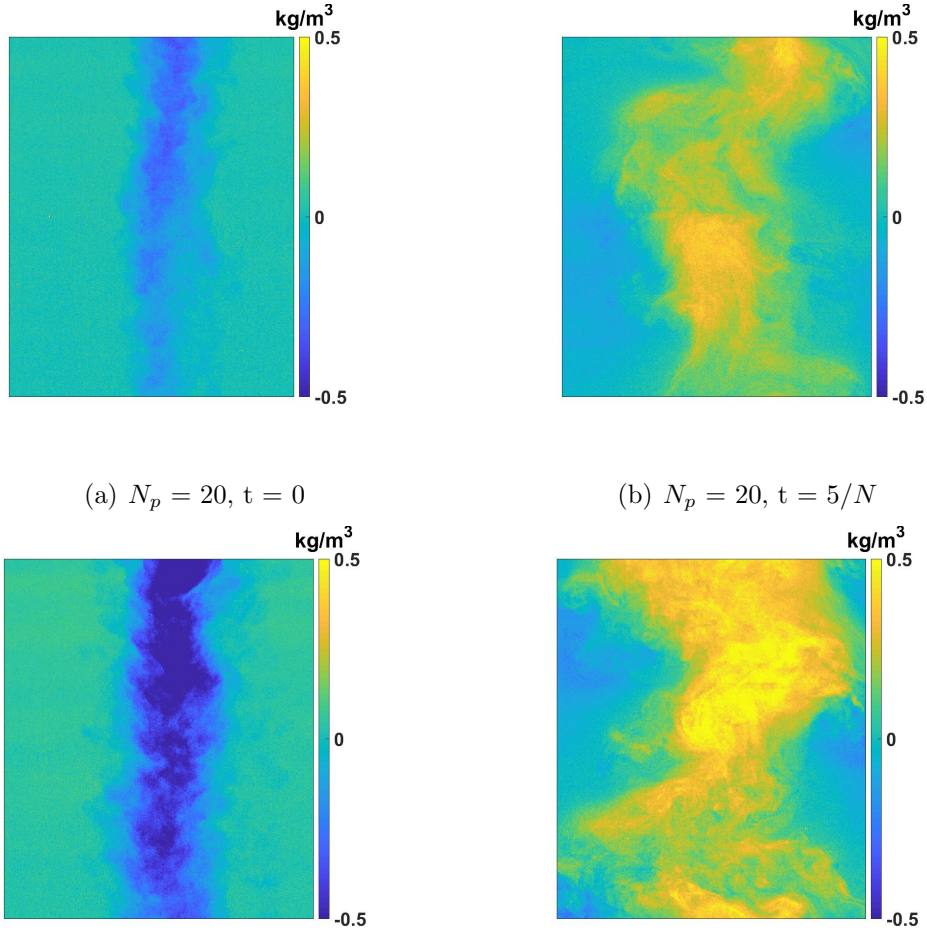

(a) $N_p = 20$, t = 0

(b) $N_p = 20$, t = $5/N$

(c) $N_p = 40$, t = 0

(d) $N_p = 40$, t = $5/N$

Fig. 3.8. Density disturbance field, N=0.37 s^{-1}, ρ_p=1405 kg/m^3

passed the field of view increases (left column in the figures). The disturbed area is an indication of the volume of light fluid dragged by the spheres. It can thus be inferred from these figures that the volume of light fluid dragged by the particles increases with N_p. This is primarily because of the total volume of the objects causing the disturbance increases with N_p. The magnitude of the disturbance increases with the density of the sphere. Also, as the magnitude of the density disturbance increases with Re and Fr, it can be inferred that the light fluid is carried to longer depths. The extent of restoration of the stratification due to buoyancy forces after 5 characteristic

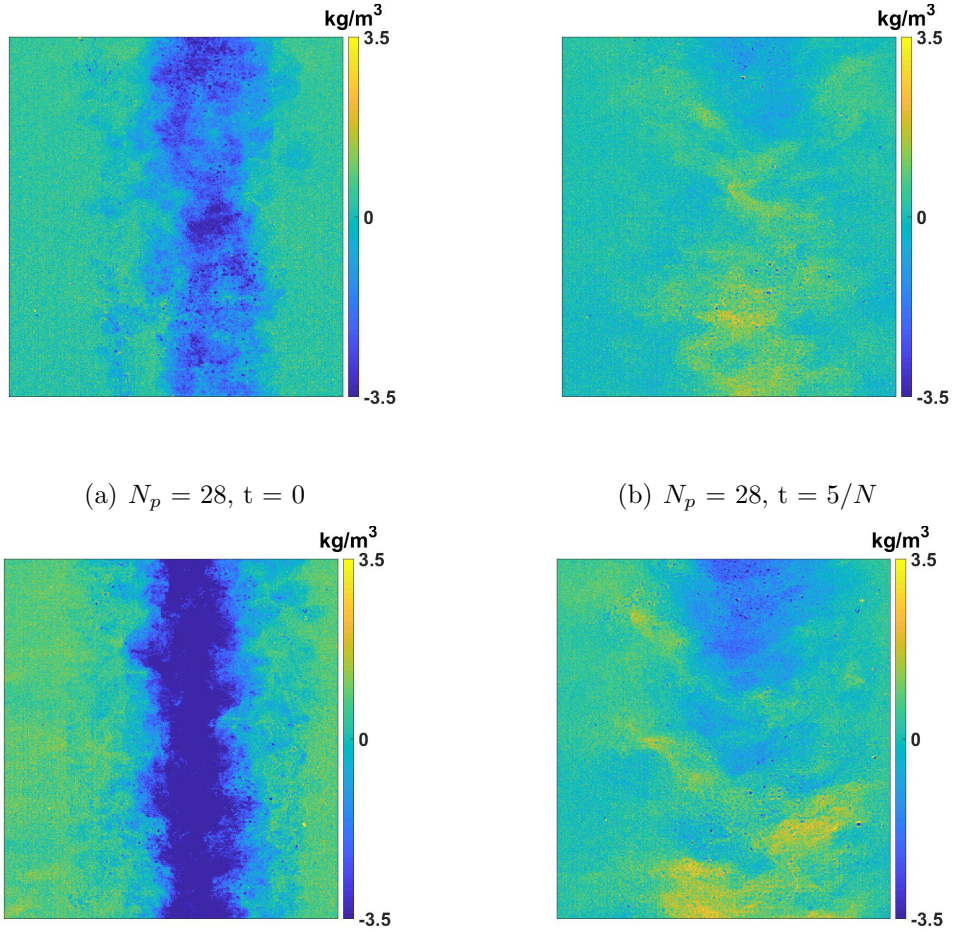

(a) $N_p = 28$, t = 0

(b) $N_p = 28$, t = $5/N$

(c) $N_p = 56$, t = 0

(d) $N_p = 56$, t = $5/N$

Fig. 3.9. Density disturbance field, N=1.22 s^{-1}, ρ_p=1405 kg/m^3

time periods can be understood from the right column of the figures. The disturbance in the system at this instant increases with N_p and Re and Fr. This is a consequence of larger volumes of light fluid being dragged in experiments with higher N_p and the magnitude of the disturbances being higher for higher Re and Fr.

Similar observations are made in Figures 3.9 to 3.11. These figures correspond to the experiments with the initial $N = 1.22\ s^{-1}$. The same stratification is used in the cylinder experiments. Hence, the number of spheres, N_p for this set of experiments

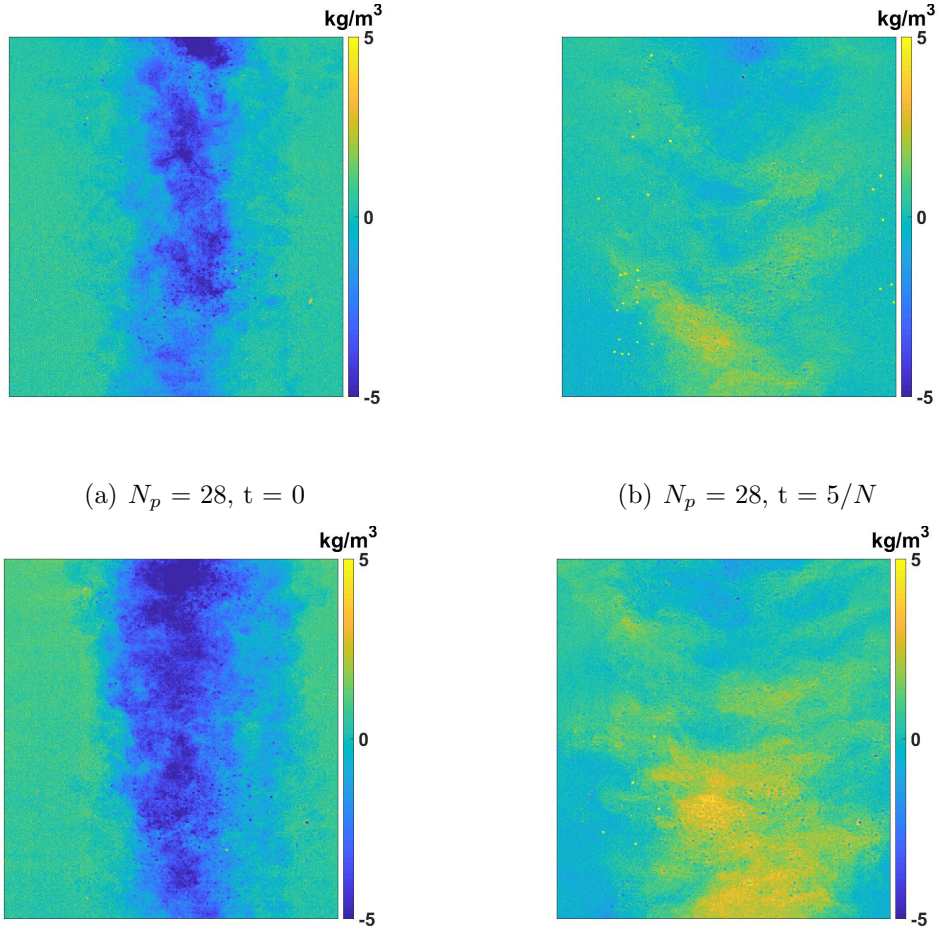

(a) $N_p = 28$, t = 0

(b) $N_p = 28$, t = $5/N$

(c) $N_p = 56$, t = 0

(d) $N_p = 56$, t = $5/N$

Fig. 3.10. Density disturbance field, N=1.22 s^{-1}, ρ_p=1805 kg/m^3

was chosen such that the total volume of the spheres was an integer multiple of the solid volume of the 1 *cm* cylinders (Figures 3.6(a) and 3.6(b)).

3.3 Perturbed volume

Particles settling in the stratified fluid transfer a certain amount of kinetic energy and drag the light fluid. After the particles have settled, the light fluid relaxes to its neutrally buoyant depth. In order to understand this process, a perturbed fluid

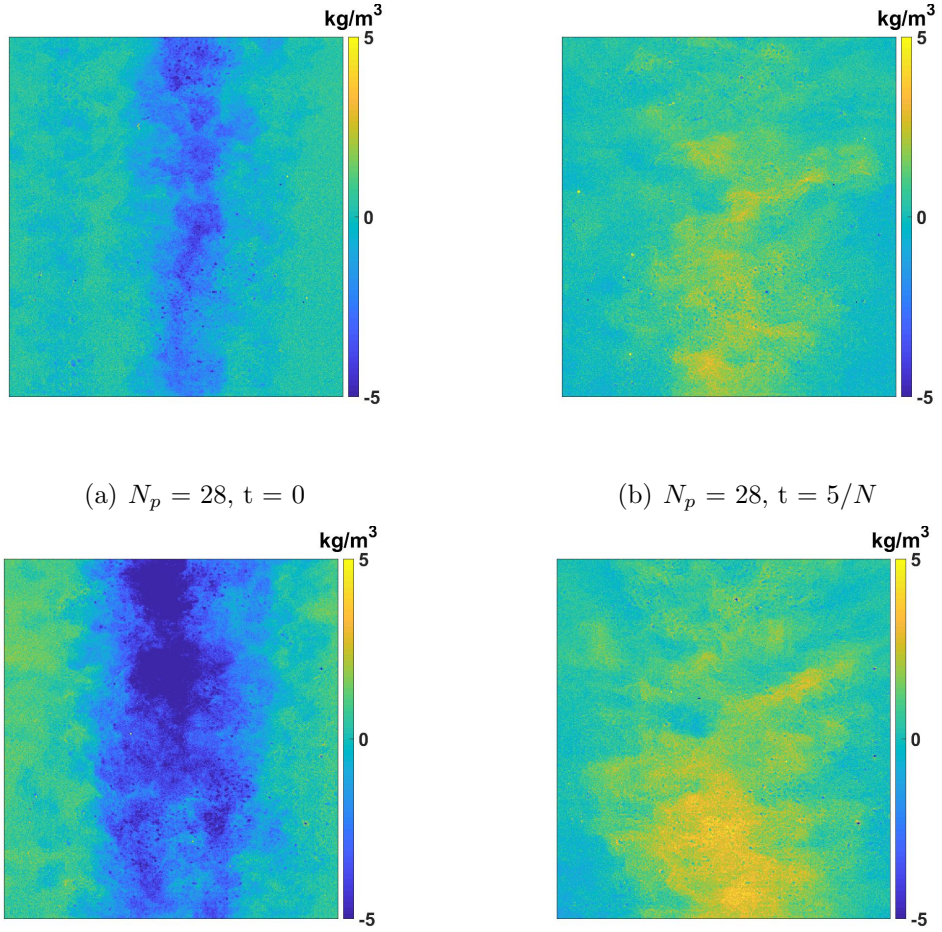

(a) $N_p = 28$, t = 0

(b) $N_p = 28$, t = $5/N$

(c) $N_p = 56$, t = 0

(d) $N_p = 56$, t = $5/N$

Fig. 3.11. Density disturbance field, N=1.22 s^{-1}, ρ_p=2091 kg/m^3

fraction (α) is defined. To calculate α at a given instant, the difference between instantaneous density field and the initial density field is calculated. α is then calculated by taking the ratio of the number of pixels with a non-zero value for the density difference to the total number of pixels in the image. The evolution of α after the particles have passed the field of view is plotted in Figures 3.12 and 3.14 for the experiments with spheres and cylinders, respectively.

Relaxation of the disturbance caused by the spheres is similar to the damped oscillation of a spring-mass system. α initially increases, reaches a maximum and

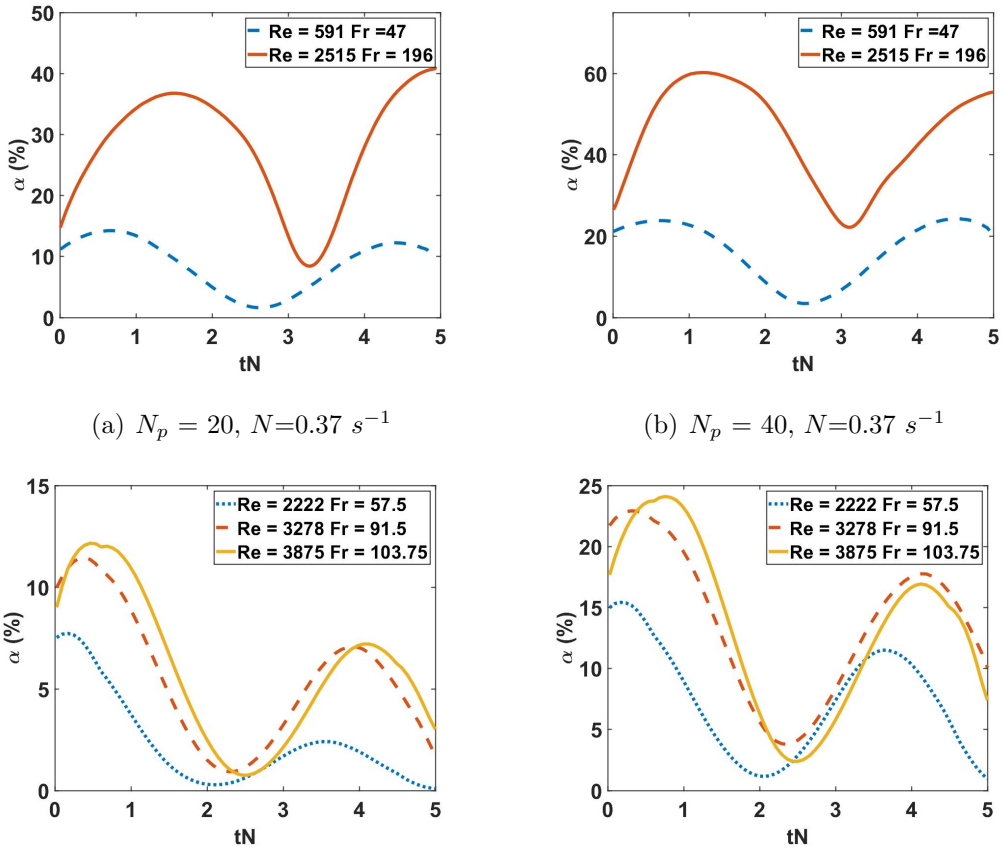

(a) $N_p = 20$, N=0.37 s^{-1}

(b) $N_p = 40$, N=0.37 s^{-1}

(c) $N_p = 28$, N=1.22 s^{-1}

(d) $N_p = 56$, N=1.22 s^{-1}

Fig. 3.12. Area perturbed by suspension of settling spheres

then decreases to a minimum. α again increases but to a value less than the previous peak and then decreases. This cycle continues with the peak decreasing in magnitude in each cycle before reducing to zero as the fluid in the tank becomes stable again. The time period of these oscillations is independent of Re and Fr. For both the stratifications, the disturbance relaxes with a time period of $3.5/N$. The first peak in the relaxation curve corresponds to the maximum initial disturbed area. The magnitude of this peak increases as Fr increases irrespective of N or N_p. It can thus be inferred that the spheres are able to disturb larger volumes of fluid with decreasing effect of stratification.

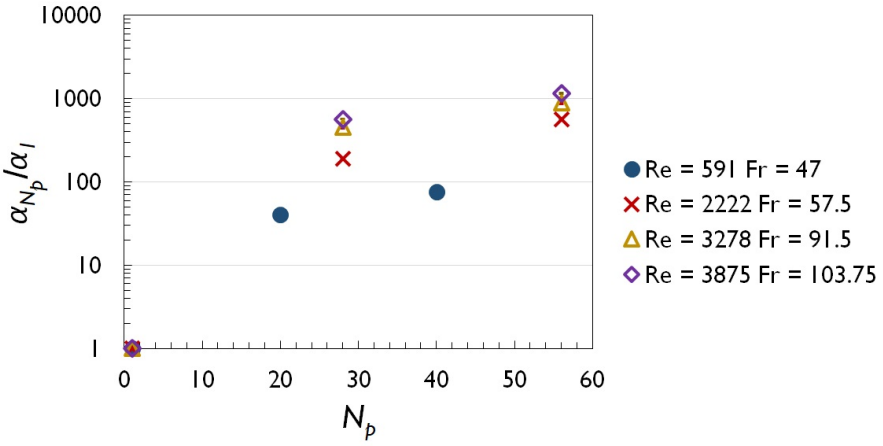

Fig. 3.13. Ratio of maximum perturbed area to the one corresponding to single particle as a function of N_p

In order to understand the effect of number of particles, fraction of the area of perturbed fluid to the one for a single sphere is plotted for different N_p number of particles. For $N_p = 20$ and $N_p = 28$, the value of α_{N_p} is not equal to α_1 times N_p. However, for a given Re and Fr, α_{N_p} for $N_p = 40$ (56) is twice the α_{N_p} for $N_p = 20$ (28).

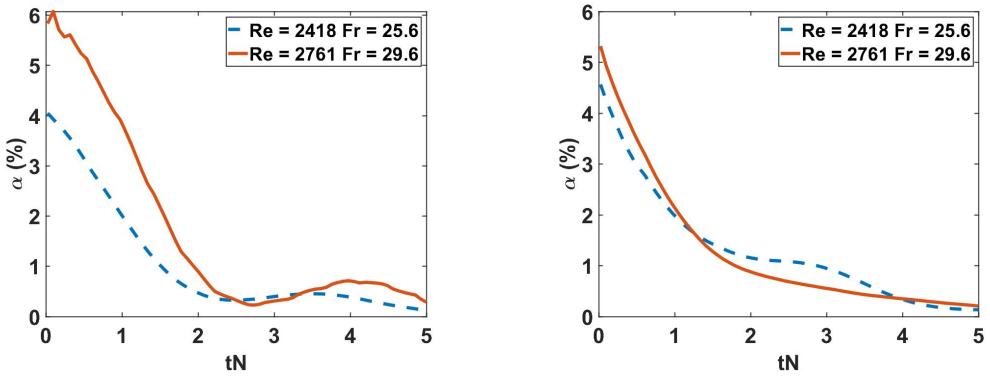

(a) $N_p = 1$ (b) $N_p = 2$

Fig. 3.14. Area perturbed by cylinder(s), d=1 cm and N=1.22 s^{-1}

The relaxation of the disturbance generated by the cylinders is different from that of the suspension of spheres. It is to be noted that a direct comparison in terms of solid volume disturbing the fluid can be made between Figures 3.14(a), 3.12(c) and Figures 3.14(b), 3.12(d). The spheres are able to disturb larger volumes of fluid when compared to the cylinders which can be seen from the magnitude of first peaks in the figures. Also, it can be seen from Figure 3.14 that the second peak in the relaxation of the disturbance is almost non-existent for the cylinders. This is because the nature of disturbance generated by the cylinders is different from the disturbance created by the spheres. The cylinders drag volumes of light fluid in their wake and shed the light fluid as vortices as they settle while the nature of the disturbance created by the spheres is displacement of volumes of light fluid. The vortices of light fluid relax at the depth they are shed by the cylinder resulting in local redistribution of the light fluid followed by local relaxation. This is illustrated in Figure 3.15. Each frame in the figure are contours of the density disturbance generated by a cylinder and are separated by $1/N$ s.

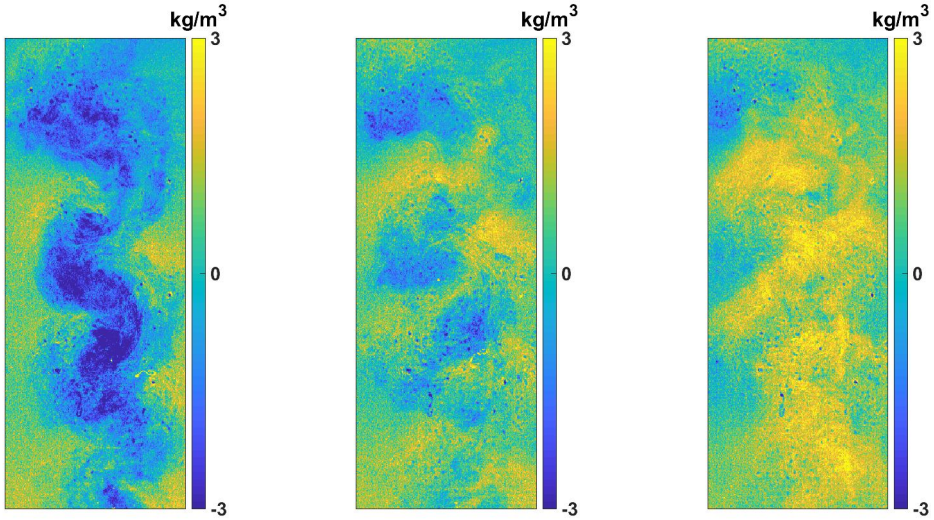

(a) t=$1/N$ (b) t=$2/N$ (c) t=$3/N$

Fig. 3.15. Relaxation of vortices shed by cylinders $Re = 2761$ $Fr = 29.6$

3.4 Potential energy and mixing

Settling spheres and cylinders push the initially stable stratification to a locally unstable state. The resulting inertial and buoyancy forces cause motion and redistribution of fluid in the tank. This leads to material surfaces of the fluid being stretched causing an effect similar to stirring. The stirred fluid may completely reverse to its original stable state through adiabatic processes or the restoration process could result in diabatic mixing of the tank. In order to quantify the extent of mixing induced by the stirring, energetics associated with the flow are analyzed. The total potential energy in the system, E_t, is divided into background potential energy E_b and the available potential energy E_a. E_b is the energy the system would have if all packets of fluid are rearranged by adiabatic sorting such that the system is reduced to a state of minimum potential energy. E_a is the amount of energy spent to adiabatically rearrange the system to this state. From this definition, when the density stratification is statically stable, the value of E_a will be zero and $E_b = E_t$. In other words, in the absence of density perturbations, the system is at its reference state and all the energy is in the form of background potential energy E_b. In the context of this study, E_a can also be interpreted as the portion of E_t in the system that is available for mixing due to the disturbances in the density field caused by the particles. The density disturbances are restored by buoyancy and during the restoration, E_a is the energy available for any form of heat or mass transfer in the system.

The density evaluated using Equation 2.2 is used to calculate the energies. Tseng & Ferziger [27] have shown that the process of evaluating a probability density function (p.d.f.) of the density of the system is equivalent to adiabatically rearranging the packets of fluid. This argument is then used to establish that, if $\rho(z)$ represents the density profile of the system, the potential energy associated with a sorted density profile $\rho(Z_r)$ calculated by evaluating the p.d.f. of $\rho(z)$ is equal to the E_b of the system. Note that Z_r is the vertical location of a packet of fluid with density ρ after

adiabatic sorting. E_t is the potential energy of the system evaluated using the actual density profile $\rho(z)$.

Let $\rho(x,z)$, H and A_c represent the density field in a given image, the height of the imaging window and the area of cross-section of the tank, respectively. The image is divided into 40 vertical strips along the x direction. This is done to account for the effect of a crests and troughs in $\rho(x)$ at a given z. A $\rho(z)$ is thus obtained in each strip by averaging $\rho(x,z)$ along x in the domain. E_b and E_t are calculated in each strip and the sum of all E_b and E_t is taken as the E_b and E_t of the system at that instant. The total potential energy, E_t is calculated as,

$$E_t = \sum_{n=1}^{N_x} \left(g A_c \int_0^H \rho(z) z dz \right) \tag{3.1}$$

where N_x is the number of vertical strips. To obtain the sorted density profile $\rho(Z_r)$ for a given strip, density calculated in each pixel in the strip is put into bins starting from ρ_m to ρ_M where ρ_m and ρ_M are the minimum and value of density in the strip. The number of pixels in each bin is then normalized using the total number of pixels in the strip to give the p.d.f. $P(\tilde{\rho})$. $P(\tilde{\rho})d\tilde{\rho}$ is the probability of getting a pixel with density ρ between $\tilde{\rho}$ and $\tilde{\rho} + d\tilde{\rho}$ in a fluid layer of thickness dZ_r and $\tilde{\rho}$ is the independent variable in the probability analysis of ρ. The volume V occupied by the fluid layer of thickness dZ_r can be related to $P(\tilde{\rho})d\tilde{\rho}$ as,

$$A_c dZ_r|_\rho = V P(\tilde{\rho}) d\tilde{\rho}|_\rho \tag{3.2}$$

The sorted height Z_r for a fluid layer of density ρ can now be calculated from the p.d.f. by integrating Equation 3.2 from ρ to ρ_M.

$$Z_r(\rho) = H \int_\rho^{\rho_M} P(\tilde{\rho}) d\tilde{\rho} \tag{3.3}$$

$Z_r(\rho)$ can be rewritten as $\rho(Z_r)$, the sorted density profile. A sample unsorted and sorted density profile is shown in Figure 3.16. E_b in the strip is the potential energy calculated using this sorted density profile. The total background potential energy of the fluid in the image is thus given by,

$$E_b = \sum_{n=1}^{N_x} g A_s \int_0^H \rho Z_r(\rho) dZ_r \tag{3.4}$$

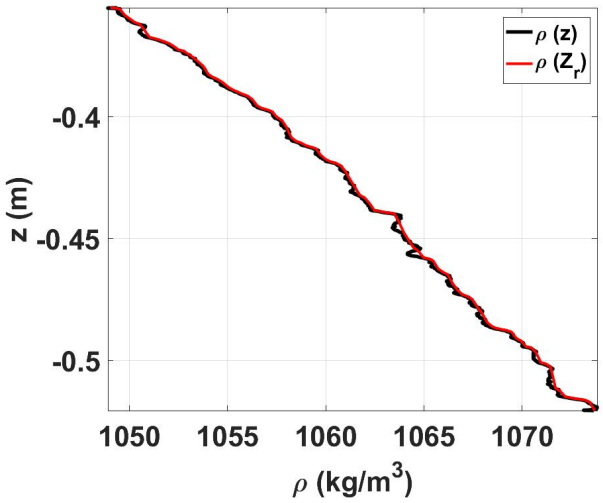

Fig. 3.16. Sample sorted and unsorted density profile

The available potential energy is calculated from E_t and E_b as,

$$E_a = E_t - E_b \tag{3.5}$$

The amount of total potential energy of the fluid converted to energy available for diabatic mixing due to the disturbances generated by the particles is thus evaluated. Figures 3.17 and 3.18 show the evolution of E_a after the particle(s) have passed the field of view. For the spheres, an oscillatory pattern similar to the evolution of α is observed. E_a generated in the system increases with decreasing Fr as the spheres disturb larger volumes of the fluid and the buoyancy forces resisting the disturbances are relatively weak. The change in E_a though does not double from $N_p = 28$ to $N_p = 56$. This is because E_a depends not only on the volume of fluid disturbed by the particles but also on the density of the disturbed volume. In Figures 3.7 - 3.11 it is seen that the magnitude of disturbance in the density field at the instant the spheres have left the field of view is 3 - 5% of the difference between the density at the top and bottom layers of fluid in the stratification while the same is 10 - 15% for the cylinders. As a result, although the cylinder does not disturb as much volume as the spheres, E_a induced by the cylinders is higher than that of the spheres (same solid

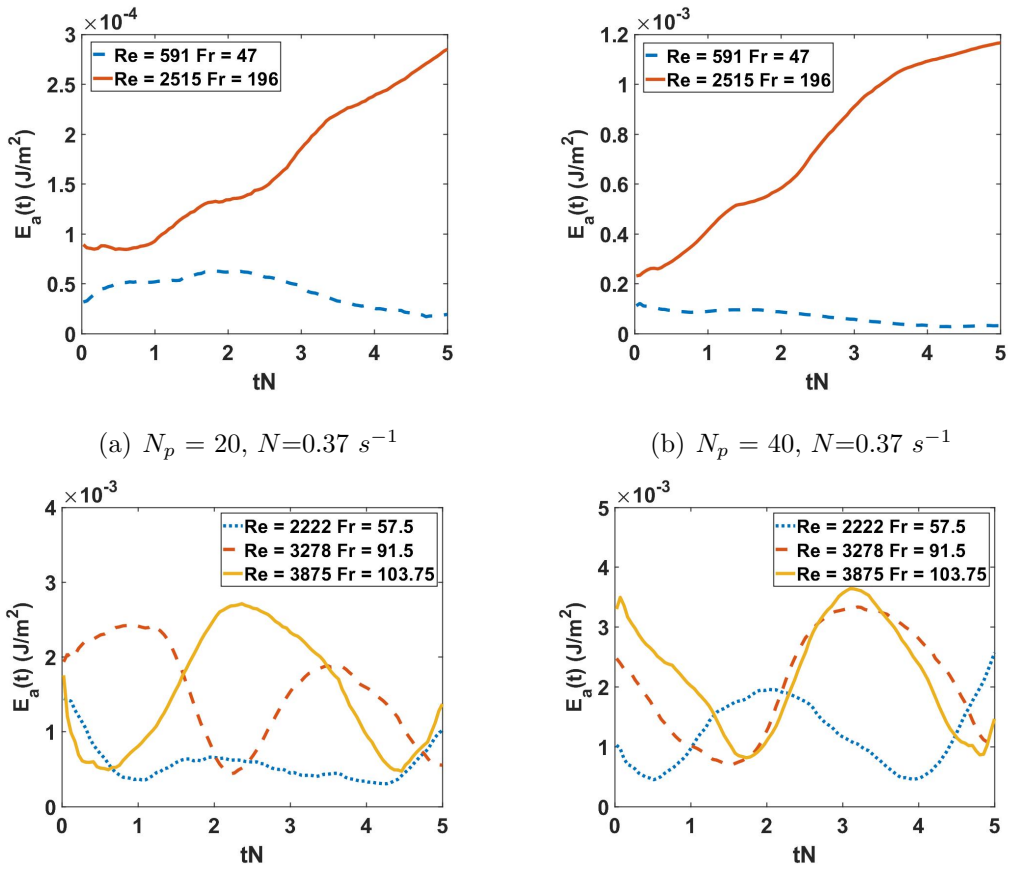

(a) $N_p = 20$, N=0.37 s^{-1}

(b) $N_p = 40$, N=0.37 s^{-1}

(c) $N_p = 28$, N=1.22 s^{-1}

(d) $N_p = 56$, N=1.22 s^{-1}

Fig. 3.17. Evolution of E_a for spheres

volume displaced by both geometries). The magnitude of the second peak in the evolution of E_a is also relatively significant compared to the first peak in E_a (Figure 3.18) while the relative magnitude of the second peak for α was very low (Figure 3.14). This is again a consequence of light fluid being dragged by the cylinder in its wake to longer depths. The transient dynamics of α and E_a provide insight to the contrasting mechanisms of generation of E_a in the system. While the spheres disturb large volumes of fluid, as the magnitude of the disturbances is smaller, E_a generated is smaller than the cylinders which create large magnitude disturbances in smaller volumes.

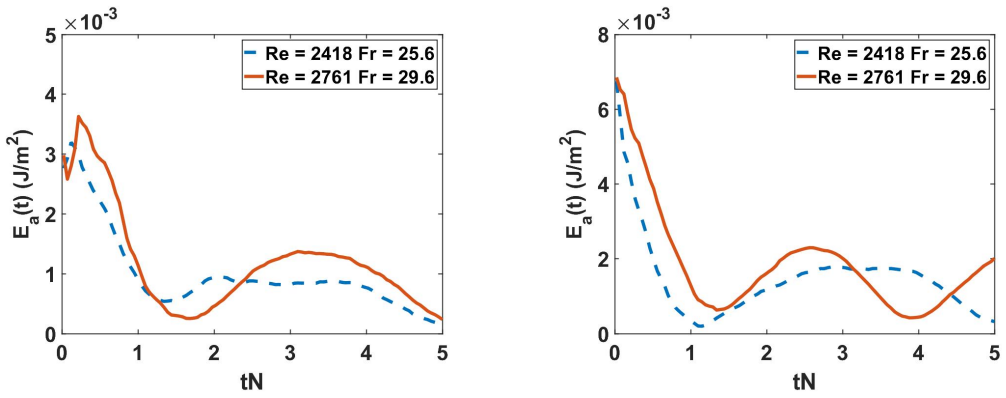

(a) $N_p = 1$ (b) $N_p = 2$

Fig. 3.18. Evolution of E_a for cylinder(s), d=1 cm N=1.22 s^{-1}

The E_a generated in the system by the particles continues to change as the displaced light fluid oscillates and decreases to zero as the system relaxes to a stable state. A portion of E_a could be used by the fluid for irreversible mixing. In order to quantify the irreversible changes to the system caused by the particles, the difference between the total potential energy of the system before and after the experiment is evaluated and an efficiency η is defined (3.6). η is the ratio of the irreversible change

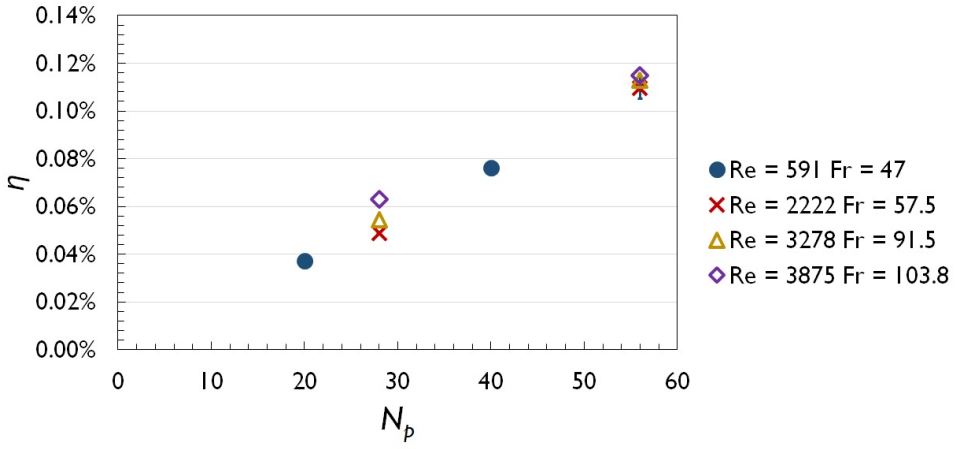

Fig. 3.19. η as a function of N_p for spheres

in potential energy caused by the particles to the total potential energy in the system before the experiment.

$$\eta = \frac{E_t(t=\infty) - E_t(t=0)}{E_t(t=0)} \tag{3.6}$$

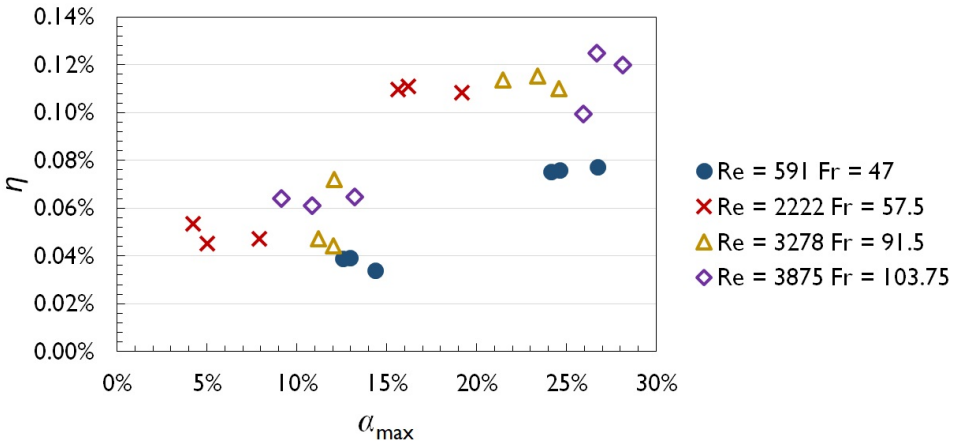

Fig. 3.20. Variation of η with α_{max} for suspension of spheres

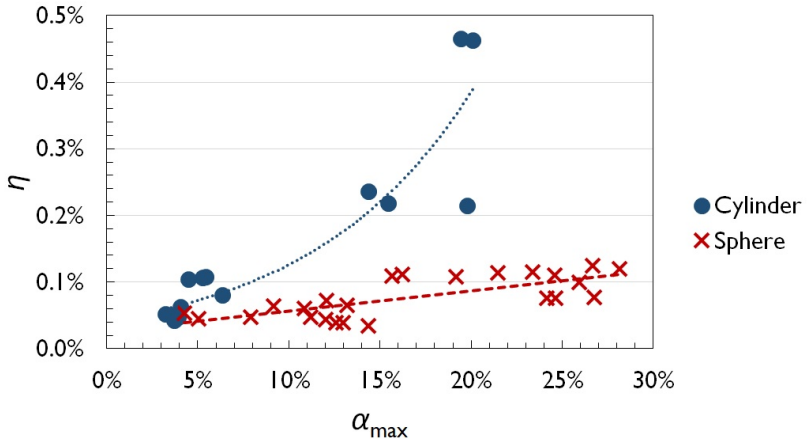

Fig. 3.21. Variation of η with α_{max} for spheres and cylinders

Figure 3.19 shows the variation of η for spheres with N_p. The ratio of change in E_t in the system increases linearly with N_p in all the cases. For any given Re and Fr, η linearly increases with α_{max} (Figure 3.20). The volume disturbed by spheres thus correlates with the amount of energy generated by the spheres which can be used for

mixing and also correlates with the irreversible change of total potential energy in the system. For cylinders with the same solid volume as spheres, the amount of E_a generated is higher even though α_{max} is lower than the spheres. This can be seen in Figure 3.21 where it is observed that η increases with α_{max} at a higher rate for cylinders than for spheres.

4. SUMMARY

Transport of particles in a stratified fluid is encountered in multiple environmental and industrial systems. Understanding the effect of stratification on transport of particles and the effect of particles on stratification is key to understanding these systems. Interaction of two different geometries of particles with stratification is studied in this work. It has been found that as the number of particles in a suspension of spheres increases, the time-average mean particle velocity reduces. The volume of fluid disturbed by the suspension increases with number of particles and Re and Fr. The volume of fluid dragged by the spheres oscillates and most of the available potential energy generated is reversibly returned to the system. The irreversible effects of the suspension of spheres are directly proportional to the volume of fluid disturbed. Hence, it can be said that for high Re and Fr, drift is a possible mechanism of mixing caused by suspensions of spheres. The disturbance caused by a cylinder is fundamentally different. The volume of fluid disturbed by the cylinder is less than that of the spheres. The light fluid dragged by the cylinders is trapped in the wake of the cylinder up-to larger depths and is released as vortices into the bulk fluid farther away from its initial location. As a result, the cylinder has larger irreversible effects to the energetics of the system. This is primarily because the rotational vortices of light fluid shed by the cylinder are more efficient than the oscillatory disturbance generated by spheres. It has been shown in the literature that the volume of fluid drifted by a particle increases with decreasing Re. As mixing is found to scale with the volume of fluid drifted by spheres, further investigation of these effects at low Re and Fr could provide further insight into stratified systems of fluid. Also, there has been little work done to characterize the wake generated by a cylinder for different values of Fr. Doing so could be a possible supplement to this work as nature of the

wake generated by cylinders plays an important role in stirring and mixing of the fluid.

REFERENCES

REFERENCES

[1] A. M. Ardekani, A. Doostmohammadi, and N. Desai, "Transport of particles, drops, and small organisms in density stratified fluids," *Physical Review Fluids*, vol. 2, no. 10, p. 100503, 2017.

[2] A. Doostmohammadi, S. Dabiri, and A. Ardekani, "A numerical study of the dynamics of a particle settling at moderate reynolds numbers in a linearly stratified fluid," *Journal of Fluid Mechanics*, vol. 750, pp. 5–32, 2014.

[3] K. Katija, "Biogenic inputs to ocean mixing," *Journal of Experimental Biology*, vol. 215, no. 6, pp. 1040–1049, 2012.

[4] S. Wang and A. M. Ardekani, "Biogenic mixing induced by intermediate reynolds number swimming in stratified fluids," *Scientific reports*, vol. 5, p. 17448, 2015.

[5] E. Bouche, V. Roig, F. Risso, and A.-M. Billet, "Homogeneous swarm of high-reynolds-number bubbles rising within a thin gap. part 1. bubble dynamics," *Journal of Fluid Mechanics*, vol. 704, pp. 211–231, 2012.

[6] C. J. Renggli, S. Wiesmaier, C. P. De Campos, K.-U. Hess, and D. B. Dingwell, "Magma mixing induced by particle settling," *Contributions to Mineralogy and Petrology*, vol. 171, no. 11, p. 96, 2016.

[7] C. Zhang, E. Churazov, and A. A. Schekochihin, "Generation of internal waves by buoyant bubbles in galaxy clusters and heating of intracluster medium," *Monthly Notices of the Royal Astronomical Society*, vol. 478, no. 4, pp. 4785–4798, 2018.

[8] J. Magnaudet and M. J. Mercier, "Particles, drops, and bubbles moving across sharp interfaces and stratified layers," *Annual Review of Fluid Mechanics*, vol. 52, 2020.

[9] C. Darwin, "Note on hydrodynamics," *Mathematical Proceedings of the Cambridge Philosophical Society*, vol. 49, no. 2, p. 342354, 1953.

[10] I. Eames, S. Belcher, and J. Hunt, "Drift, partial drift and darwin's proposition," *Journal of Fluid Mechanics*, vol. 275, pp. 201–223, 1994.

[11] J. Zhang, M. J. Mercier, and J. Magnaudet, "Core mechanisms of drag enhancement on bodies settling in a stratified fluid," *Journal of Fluid Mechanics*, vol. 875, pp. 622–656, 2019.

[12] A. Ardekani and R. Stocker, "Stratlets: Low reynolds number point-force solutions in a stratified fluid," *Physical review letters*, vol. 105, no. 8, p. 084502, 2010.

[13] C. Torres, H. Hanazaki, J. Ochoa, J. Castillo, and M. Van Woert, "Flow past a sphere moving vertically in a stratified diffusive fluid," *Journal of Fluid Mechanics*, vol. 417, pp. 211–236, 2000.

[14] H. Hanazaki, K. Konishi, and T. Okamura, "Schmidt-number effects on the flow past a sphere moving vertically in a stratified diffusive fluid," *Physics of Fluids*, vol. 21, no. 2, p. 026602, 2009.

[15] H. Hanazaki, S. Nakamura, and H. Yoshikawa, "Numerical simulation of jets generated by a sphere moving vertically in a stratified fluid," *Journal of Fluid Mechanics*, vol. 765, pp. 424–451, 2015.

[16] D. Mowbray and B. Rarity, "The internal wave pattern produced by a sphere moving vertically in a density stratified liquid," *Journal of Fluid Mechanics*, vol. 30, no. 3, pp. 489–495, 1967.

[17] H. Hanazaki, K. Kashimoto, and T. Okamura, "Jets generated by a sphere moving vertically in a stratified fluid," *Journal of Fluid Mechanics*, vol. 638, pp. 173–197, 2009.

[18] S. Okino, S. Akiyama, and H. Hanazaki, "Velocity distribution around a sphere descending in a linearly stratified fluid," *Journal of Fluid Mechanics*, vol. 826, pp. 759–780, 2017.

[19] K. Y. Yick, C. R. Torres, T. Peacock, and R. Stocker, "Enhanced drag of a sphere settling in a stratified fluid at small reynolds numbers," *Journal of Fluid Mechanics*, vol. 632, pp. 49–68, 2009.

[20] R. Chadwick and Y. Zvirin, "Slow viscous flow of an incompressible stratified fluid past a sphere," *Journal of Fluid Mechanics*, vol. 66, no. 2, pp. 377–383, 1974.

[21] A. Doostmohammadi and A. Ardekani, "Interaction between a pair of particles settling in a stratified fluid," *Physical Review E*, vol. 88, no. 2, p. 023029, 2013.

[22] J. W. Bush, B. Thurber, and F. Blanchette, "Particle clouds in homogeneous and stratified environments," *Journal of Fluid Mechanics*, vol. 489, pp. 29–54, 2003.

[23] A. Doostmohammadi and A. Ardekani, "Suspension of solid particles in a density stratified fluid," *Physics of Fluids*, vol. 27, no. 2, p. 023302, 2015.

[24] E. N. Lorenz, "Available potential energy and the maintenance of the general circulation," *Tellus*, vol. 7, no. 2, pp. 157–167, 1955.

[25] F. Blanchette, "Mixing and convection driven by particles settling in temperature-stratified ambients," *International Journal of Heat and Mass Transfer*, vol. 56, no. 1-2, pp. 732–740, 2013.

[26] G. Oster, "Density gradients," *Scientific American*, vol. 213, no. 2, pp. 70–79, 1965.

[27] Y.-h. Tseng and J. H. Ferziger, "Mixing and available potential energy in stratified flows," *Physics of Fluids*, vol. 13, no. 5, pp. 1281–1293, 2001.

APPENDIX

A. UNCERTAINTY CALCULATIONS

If ∂ indicates partial derivative and $\Delta\rho^0$, ΔA, ΔB, ΔC, ΔI_0 and ΔI are the absolute uncertainties in $\rho^0 A, B$, C, I_0 and I respectively, the relative uncertainty in density, $\Delta\rho/\rho$ can be estimated by applying Taylor's formula for uncertainty on Equation 2.2.

$$\frac{\Delta\rho}{\rho} = \left\{ \left(\frac{\partial\rho}{\partial\rho_0}\right)^2 \left(\frac{\Delta\rho_0}{\rho}\right)^2 + \left(\frac{\partial\rho}{\partial I_0}\right)^2 \left(\frac{\Delta I_0}{\rho}\right)^2 + \left(\frac{\partial\rho}{\partial I}\right)^2 \left(\frac{\Delta I}{\rho}\right)^2 + \left(\frac{\partial\rho}{\partial A}\right)^2 \left(\frac{\Delta A}{\rho}\right)^2 + \left(\frac{\partial\rho}{\partial B}\right)^2 \left(\frac{\Delta B}{\rho}\right)^2 + \left(\frac{\partial\rho}{\partial C}\right)^2 \left(\frac{\Delta C}{\rho}\right)^2 \right\}^{0.5} \tag{A.1}$$

Evaluating individual terms in Equation A.1 using Equation 2.2,

$$\frac{\partial\rho}{\partial\rho_0} = 1 \tag{A.2}$$

$$\frac{\partial\rho}{\partial I_0} = \frac{1}{I_0\tilde{R}} \tag{A.3}$$

$$\frac{\partial\rho}{\partial I} = \frac{-1}{I\tilde{R}} \tag{A.4}$$

$$\frac{\partial\rho}{\partial A} = \frac{\ln(I_0) - \ln(I) + C}{A\tilde{R}} - \frac{-B - \tilde{R}}{2A^2} \tag{A.5}$$

$$\frac{\partial\rho}{\partial B} = \frac{-B - \tilde{R}}{2A\tilde{R}} \tag{A.6}$$

$$\frac{\partial\rho}{\partial C} = \frac{1}{\tilde{R}} \tag{A.7}$$

where $\tilde{R}$ is $\left(\sqrt{B^2 - 4A\left(C - \ln I + \ln I_0\right)}\right)$. The absolute uncertainty in ρ is evaluated by multiplying $\Delta\rho/\rho$ with the evaluated density field from Equation 2.2